Optimum Combining of Handset Diversity Antennas

by

Peter Mawusi Yautse Agboh

Submitted to the Department of Electrical Engineering and Computer Science

in partial fulfillment of the requirements for the degree of

Master of Engineering in Computer Science and Engineering

at the

MASSACHUSETTS INSTITUTE OF TECHNOLOGY

May 2001

Author .....
Department of Electrical Engineering and Computer Science
April 2, 1990

Certified by .....
Mike Wengler
Doctor
VI-A Thesis Supervisor

Certified by .....
Jin Au Kong
Professor
M.I.T Thesis Supervisor

Accepted by .....
Arthur C. Smith
Chairman, Department Committee on Graduate Students

Optimum Combining of Handset Diversity Antennas

by

Peter Mawusi Yautse Agboh

Submitted to the Department of Electrical Engineering and Computer Science
on April 2, 1990, in partial fulfillment of the
requirements for the degree of
Master of Engineering in Computer Science and Engineering

Abstract

In this thesis cellular handset and mobile terminal forward link sensitivity improvements due to dual-antenna systems with smart-antenna combining algorithms were determined. The performance of a mobile handset with a top-mounted monopole and back-mounted internal monopole was determined in the field. Handset field tests were conducted both for the handset attached to a phantom-head model and held by a human operator so that the effect of hand blockage and coupling were measured. The measurements were made on the IS-95 (CDMA) SPRINT PCS system in various parts of San Diego. Logged data was analyzed for single antenna performance, selection diversity combining, maximum ratio combining, and optimum combining.

VI-A Thesis Supervisor: Mike Wengler
Title: Doctor

M.I.T Thesis Supervisor: Jin Au Kong
Title: Professor

Acknowledgments

I would like to express my appreciation to M.I.T Professor Jin Au Kong for the level of independence he allowed me in my thesis. His patience, advice, and supervision as the MIT side of my thesis is appreciated.

I wish also to express my appreciation to Doctor Mike Wengler of Qualcomm Inc. for giving me the opportunity to work with him in such an exciting field. His mentorship, motivation, and direction has taken me a long way. Dr Wengler was also responsible for much of the DSP code used in detecting, and de-spreading the CDMA signals.

The entire Research and Development division of Qualcomm Inc. in San Diego whose individual names are too numerous to mention deserve acknowledgement for their support. Randy Standke of Qualcomm Inc. deserves special mention for his assistance in collecting the dual antenna field data.

Finally I thank my parents, my brother Charles, my sisters Evelyn and Bridgitte for whose support and encouragement I am truly gratefull.

Peter M. Y. Agboh

Cambridge, Massachusetts

Contents

List of Figures

List of Tables

Chapter 1

Overview

1.1 Introduction

Antenna Diversity has been recognized since the invention of cellular telephony as an effective way to improve the typical mobile radio channel ([10], [11]). Since the first deployment of commercial cellular systems, dual-antenna diversity receivers have been utilized at the base station to enhance the reverse link.

The use of multiple antennas on handsets to improve signal reception in the forward link has been retarded by two reasons 1) the over-all cost and complexity of implementation at every mobile are much greater than that of implementing only at each base station; 2) whereas conventional space-diversity ([10], [4]) suggests that de-correlated signals for use in a spatial diversity system are restricted only by adequately large antenna separations (on the order of several wavelengths) [2], the compact and almost miniature size of handsets are of the order of a wavelength. With experimental results of Vaughan, Tsunekawa, Gaggioli, Colsburn, Leather and Sash ([13], [8], [7], [5], [9], [12]) suggesting a lower than predicted correlation in handset antennas, availability of high performance digital signal processing components, and increasing demands on the available spectrum, the wireless industry is showing a surge of interest in antenna diversity on the forward link.

To this date there has been considerable research on forward link sensitivity improvements using multiple antennas on the handset. However, to my knowledge no study has yet been dedicated to cellular handset and mobile terminal forward link sensitivity improvements due to dual-antenna systems using Optimum Combining (OC) in a commercially deployed IS-95 system.

In this thesis, the cellular handset forward link sensitivity improvements due to dual-antenna systems with smart-antenna combining algorithms were determined. The performance of a mobile handset with a top-mounted monopole and back-mounted internal monopole was determined in the field. Handset field tests were conducted both for the handset attached to a phantom-head model and held by a human operator so that the effect of hand blockage and coupling were analyzed. The measurements were made on the IS-95 (CDMA) SPRINT PCS system in various parts of San Diego. Logged data was analyzed and OC was compared with single antenna performance, Selection Diversity (SD) combining, Maximum Ratio Combining (MRC).

Experiments performed by Leather, Braun and Bonaccorso are closest to this study ([9], [3], and [2]) . Leather's experiment differs from this study in that dual antenna SINR gains were evaluated indirectly in terms of the cross correlation coefficients [9]. The report used SD, MRC, and OC combining schemes to give direct estimates of signal-to-interference and noise ratio (SINR) improvements. In this study data was collected under real-life mobile conditions whereas measurements done by Braun were in a controlled laboratory environment using a maximum of two interference signals [3]. Bonaccorso performed simulations on the SINR improvements using OC combining on the mobile handset in a CDMA high data rate communication system [2]. Bonaccorso's simulations considered SINR improvement losses due to parameter estimation errors [2]. This study incorporates the results obtained by Bonaccorso and goes further by applying OC to a commercially deployed IS-95 system where the parameter estimations errors are incorporated into the results [2].

1.2 Report Outline

Here, the organization of this report is explained. Chapter two introduces diversity antenna systems: the definition of a diversity antenna system is given and the concepts of spatial diversity and interference reduction are described. Then the optimum solution for various diversity antenna performance criteria are derived. The chapter concludes with an analysis of how spatial diversity and interference reduction is affected by the cross correlation of signals at the two antennas; this is a function of the propagation environment wherein the diversity antenna system is operating.

Chapter three provides a brief description of the IS-95 forward link physical layer. A brief technical overview of the IS-95 standard is given followed by a description of the forward link transmitter and forward link channels.

The measurement system is described in Chapter four. Parameter estimation, used to generate the complex weights for signal combining, and signal-to-interference-and-noise (SINR) estimation at the combiner output are presented. Limitations in parameter estimation and their impact on the results are discussed.

In chapter five, diversity antenna measurements are presented. Data were collected in three different channel environments and the extent of multi-path and interference are examined. The SINR at the combiner output using Optimum Combining (OC) is compared with that of Selective Diversity (SD) and Maximum Ratio Combining (MRC). The effects of operator's hand blockage on the diversity antenna system is also investigated.

Finally, Chapter six concludes this report with a summary of the results and suggestions for further research.

Chapter 2

Introduction to Diversity Antenna Systems

In this chapter the fundamentals of diversity antennas are covered. First, a signal model for diversity antennas is presented; then, spatial diversity and interference cancellation is discussed. After that, linear optimum performance solutions for adaptive combining are investigated; finally, the dependence of the output SINR of MRC and OC on the cross correlation properties of the propagation environment is analyzed.

2.1 Definition

A diversity antenna system is a multi-antenna system composed of a collection of spatially separated antenna elements whose output is combined using some scheme. (Figure 2-1 shows such an antenna system). What distinguishes a multi-antenna system from a single antenna receiver is that the former has the capability to dynamically adjust the combining mechanism so as to improve system performance and/or capacity; such systems are usually termed adaptive. In this report the difference between an adaptive system and a diversity system is blurred; both are at-times referred to as diversity systems. This is because a diversity system can be transformed to an adap-

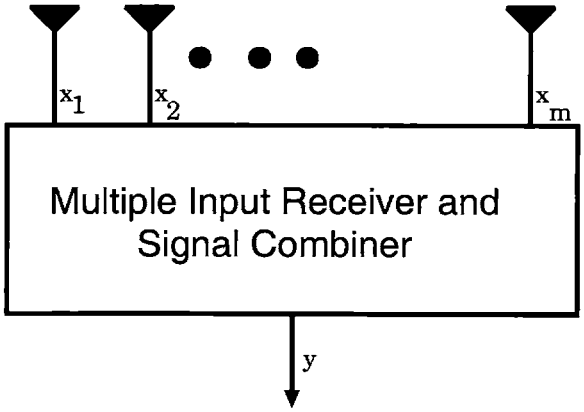

Figure 2-1: Diversity antenna system with multiple input receiver and signal combiner

tive one by alternating its combining mechanism; It is the way in which the signals at the antenna elements are combined that distinguishes an adaptive system from a diversity one. Both utilize multiple antenna elements and combine the received signal in some way.

2.2 Spatial Diversity and Interference Cancellation

The term spatial diversity refers to diversity antenna systems whose primary goal is to mitigate multi-path fading which arises in scattering environments. In environments where scattering occurs, the signal present at any point is a sum of various components that have traveled along different paths from source to destination. (See figure 2-2). Since the lengths of these paths are not necessarily the same, the various signal components arrive at the receiver with random phases. The multi-path components of the signal may combine either coherently or destructively. When the signal components combine destructively the received signal power may be extremely low; the signal is said to have undergone a multi-path fade. In figure 2-2, the received signal from sector 2 at antenna 1 is $(c(1,1)+c(1,2)+c(1,3))\,s$ where $c(1,i)$ is the complex path gain of sector 2's signal along path i at antenna 1. Multi-path fading is due to the fact that $|c(1,1)+c(1,2)+c(1,3)|^2$ may be very small.

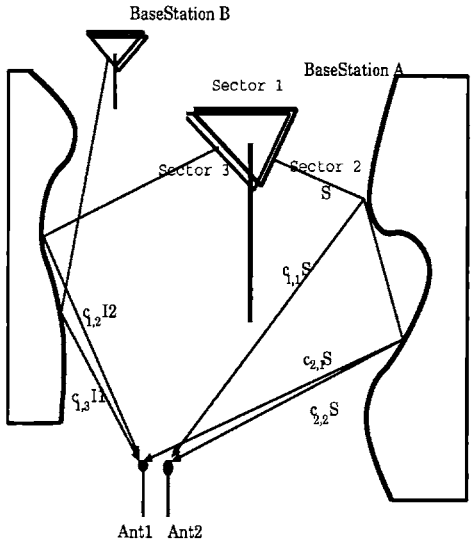

Figure 2-2: Multi-path propagation in scattering environment

Spatial diversity systems use multiple antennas separated in space to mitigate multi-path fading. Because the multi-path signal components have random phases, it is unlikely that at any particular instant the signal fades at all the receiver antennas. There usually is, therefore, good signal reception on at least one of the diversity antennas. The received signal may then be combined to maximize the desired signal power in the presence of noise and interference, or noise alone.

The degree by which any spatial diversity system is able to combat multi-path fading depends on the cross-correlation of the fading signal envelopes and the mean signal powers, observed at the various antenna elements. The smaller the cross-correlation, the more likely that signal fades do not coincide at all the antenna elements and the higher the diversity gain. Diversity gains decrease when significant differences exist in mean signal power at the antenna elements. The extreme case is when the mean signal at one branch is much larger than that of the other antennas; then, the antenna elements receiving weaker signal power do not suffice as an alternative to receive the desired signal. In this situation the diversity antenna system effectively acts like a single receiver. Hence, gains from using diversity systems are reduced when significant differences exist in the mean signal power levels at the different antennas.

Spatial diversity system performances depend also on the cross correlation of inter-

ference at the antennas. In diversity systems it is normally desired that interference should not be correlated at the antenna; it should be noise-like. Thus it is usually assume that interfering signals at the different antenna terminals are not correlated. This assumption is valid if the antenna terminals are spaced far enough apart. For a base station this condition is readily fulfilled by placing the antennas at least 7λ apart [10]; the equivalent spacing requirement for de-correlated signals at the handset is at least 0.2λ [10]. To place handset antennas any closer would make interference correlated and reduce the performance of the diversity system. In the presence of correlated interference, maximizing signal power and reducing interference in the pretense of noise is desirable; thus, interference reduction or cancellation is sought alongside mitigation of multi-path fading. It is for this reason that Optimal Combining is of special interest to this report.

Below is presented brief descriptions of SD, EGC, MRC, and OC. The description of SD, MRC and OC provide background for how SD, OC and MRC are implemented. A description of EGC is included for completeness.

2.2.1 Signal Model

Let

- s is the transmitted signal
- M be the number of antennas used in the diversity antenna system
- $\mathbf{c} = [\sum_j c_{j,1}, \sum_j c_{j,2}, ..., \sum_j c_{j,M}]^T$ be the vector of the complex fading coefficients of the received multi-path components at the M antennas. $c_{j,i}$ is the complex fading coefficient for the signal paths indexed by i on antenna j
- $\mathbf{x} = [x_1, x_2, ..., x_M]^T$ be the vector of received signal plus noise plus interference at each of M antennas
- $\mathbf{w} = [w_1, w_2, ..., w_M]^T$ be the vector of the combining weights as applied at each of M antennas

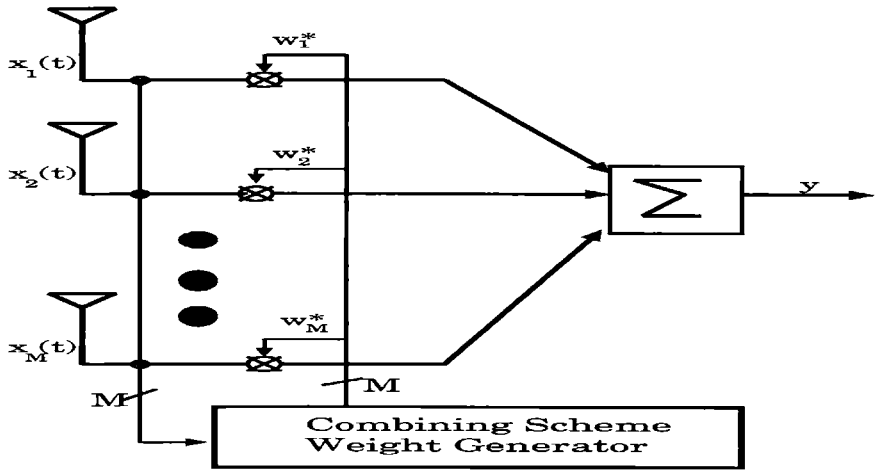

Figure 2-3: Signal combining at diversity antennas

- $\mathbf{n} = [n_1, n_2, ..., n_M]^T$ be the vector containing the zero mean noise plus interference such that $\nabla_{i,j \neq i} E\left[n_i n_j^*\right]$ is not necessarily equal to zero.

Assuming the received signal is of form

$$x_m = \sum_j c_{j,m} s + n_m \tag{2.1}$$

From figure 2-3 output of the diversity antenna system's combiner

$$y = \sum_{1 \leq i \leq M} w_i^* x_i \tag{2.2}$$

or in matrix notation,

$$y = \mathbf{w}^H \mathbf{x}. \tag{2.3}$$

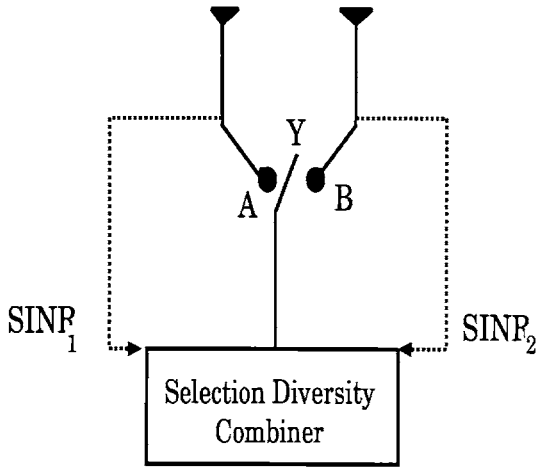

Figure 2-4: Selection diversity combiner

2.2.2 Selection Diversity (SD)

In selection diversity, the receiver estimates the signal-to-noise ration (SNR), at each antenna element and at each time episode, selects as output signals received from the single antenna with the largest instantaneous SNR. (Figure 2-4 illustrates the SD combiner). It is equivalent to a motored switch that after every T seconds, determines whether $SNR_1 > SNR_2$ and positions the point Y at A if the condition is met; otherwise, Y is at B. Mathematically the operations of the SD combiner are equivalent to applying at antenna i the weights

$$w_{i,SD} = \begin{cases} 1 \text{ if } SNR_i = MAX\{SNR_1, SNR_2, ..., SNR_M, \\ 0 \text{ otherwise} \end{cases}$$

2.2.3 Equal Gain Combining (EGC)

In EGC the receiver first co-phases the desired signal components at each antenna and adds the co-phased signals together. EGC maximizes SNR only when the noise power is equal at the antenna elements. The EGC weight at each antenna is

$$w_{i,EGC} = c_{desired-signal,i}$$

2.2.4 Maximum Ratio Combining (MRC)

The receiver implementing MRC multiplies the received signal at each antenna with the instantaneous SNR on that branch. MRC seeks to maximize the SNR of the desired signal in the presence of white noise (which may be of unequal power at each antenna). MRC is identical to EGC when noise power is the same for all antenna elements. When the noise is white but noise power is different at some of the antenna elements, MRC is an optimal combining scheme. If σ_s^2 is the transmitted signal power and $\sigma_{i,n}^2$ is the noise plus interference power at antenna i, the MRC weight at antenna i is

$$w_{i,MRC} = c_{desired-signal,i}\frac{\sigma_s}{\sigma_{i,n}}$$

2.2.5 Optimum Combining (OC)

The derivation of weights for OC is provided below. OC seeks to maximize the SINR of some desired signal. It is identical to MRC when the noise and interference are both white. In the presence of correlated interference, OC will seek to reduce the interference power and maximize SNR.

2.3 Optimum Performance Criteria

The following sections explain how the received signal at each antenna element is combined to produce the OC combiner output. This section also proves that the SINR

at the output of the OC combiner is optimum under minimum-mean-square-error, linearly constrained minimum variance, maximum signal-to-interference and noise ratio, and maximum likelihood performance criteria. The derivations are identical to that of Ertel and Bonaccorso ([6], [2]).

2.3.1 Minimum Mean Square-Error (MMSE)

One possible performance criterion is minimization of the squared error between the combiner output y and some desired signal s. The goal is to select the antenna weight vector $\mathbf{w}$ which minimize the squared error:

$$\begin{aligned} J(\mathbf{w}) &= E\left[|d-y|^2\right] = E\left[\left|d-\mathbf{w}^H\mathbf{x}\right|^2\right] \\ &= E\left[\left(d-\mathbf{w}^H\mathbf{x}\right)\left(d-\mathbf{w}^H\mathbf{x}\right)^H\right] = E\left[dd^H-(\mathbf{x}d^H)^H\mathbf{w}-\mathbf{w}^H\mathbf{x}d^H+\mathbf{w}^H\mathbf{x}\mathbf{x}^H\mathbf{w}\right] \end{aligned}$$

The mean squared error is minimized when the gradient of $J(\mathbf{w})$ becomes zero. ie.,

$$\nabla_w J(\mathbf{w}) = E\left[-d^H\mathbf{x}+\mathbf{x}\mathbf{x}^H\mathbf{w}\right] = 0$$

which when solved yields

$$\mathbf{w} = \left(E\left[\mathbf{x}\mathbf{x}^H\right]\right)^{-1}E\left[d^H\mathbf{x}\right] \tag{2.4}$$

If we define $\mathbf{R}_{xx} = E\left[\mathbf{x}\mathbf{x}^H\right]$, the correlation matrix of $\mathbf{x}$, and and $\mathbf{r}_{xs} = E\left[s^H\mathbf{x}\right]$, the correlation of received signal with the desired signal, then equation 2.4 may be rewritten as

$$\mathbf{w}_{MMSE} = \mathbf{R}_{xx}^{-1}\mathbf{r}_{xd} \tag{2.5}$$

This result is the Optimum MMSE solution and is commonly called the Wiener-Hopf equation or the Wiener solution. The solution is first generalized, in order to show that all the performance criteria lead to the same optimum SINR solution. Let the received signal be represented by

$$\mathbf{x} = \mathbf{c}s + \mathbf{n} \tag{2.6}$$

If the desired signal is orthogonal to the interference and noise,ie: $\nabla_i E\left[sn_i\right] = 0$ then $\mathbf{R}_{xx}$ and $\mathbf{r}_{xd}$ may be expressed as

$$\mathbf{R}_{xx} = \mathbf{R}_{nn} + \sigma_s^2\mathbf{c}\mathbf{c}^H \tag{2.7}$$

$$\mathbf{r}_{xd} = E\left[(\mathbf{c}s + \mathbf{n})s*\right] = \sigma_s^2\mathbf{c} \tag{2.8}$$

Where $\mathbf{R}_{nn} = E\left[\mathbf{n}\mathbf{n}^H\right]$ is the interference plus noise cross-correlation matrix and $\sigma_s^2 = E\left[|s|^2\right]$ is the desired signal's power at the transmitter.

By the matrix inversion lemma:

$$\mathbf{R}_{xx}^{-1} = \mathbf{R}_{nn}^{-1} - \sigma_s^2\frac{\mathbf{R}_{nn}^{-1}\mathbf{c}\mathbf{c}^H\mathbf{R}_{nn}^{-1}}{1 + \sigma_s^2\mathbf{c}^H\mathbf{R}_{nn}^{-1}\mathbf{c}} \tag{2.9}$$

This expression can be simplified by defining the constant $k = \sigma_s^2\mathbf{c}\mathbf{R}_{nn}^{-1}\mathbf{c}$; equation 2.5 simplifies to

$$\mathbf{w_{MMSE}} = \frac{1}{1+k}\mathbf{R}_{nn}^{-1}\mathbf{r}_{xd} = \beta_{MMSE}\mathbf{R}_{nn}^{-1}\mathbf{c} \tag{2.10}$$

Where $\beta_{MMSE} = \frac{1}{1+\sigma_s^2\mathbf{c}^H\mathbf{R}_{nn}^{-1}\mathbf{c}}$. Since the weight $\mathbf{w}$ is applied to the desired signal as well as the interference and noise, its magnitude need not be maintained; thus,

$$\mathbf{w}' = \mathbf{R}_{nn}^{-1}\mathbf{r}_{xd} \tag{2.11}$$

or

$$\mathbf{w}'' = \mathbf{R}_{nn}^{-1}\mathbf{c} \tag{2.12}$$

Although equations 2.5 and 2.12 are equivalent in theory, their performance in practice may differ due to different estimation errors - in the real world the autocorrelation matrices must be estimated. Bonaccorso presented simulation results that showed that at the 0-40Mph speeds in Rayleigh Fading, the SINR at the output of the OC combiner when the weights are generated using $\mathbf{R}_{xx}$, is less than when the OC weights are generated using $\mathbf{R}_{nn}$ [2]. This is because more estimated parameters are used in equation 2.5; its estimation errors are expected to be larger than those of equation 2.11 or 2.12. In this thesis, therefore, an approximation of 2.12 is employed.

2.3.2 Linearly Constrained Minimum Variance (LCMV)

Using 2.6 gives an expression for the signal at the optimum combiner output

$$y = \mathbf{w}^H\mathbf{x} = \mathbf{w}^H\mathbf{c}s + \mathbf{w}^H\mathbf{n} \tag{2.13}$$

If the output of the optimum combiner filer is constrained such that $\mathbf{w}^H\mathbf{c} = G$ (where

if $G = 1$ then y is an unbiased estimate of the desired signal. ie., $E[y] = d$), then

$$y = Gd + \mathbf{w}^H \mathbf{n} \tag{2.14}$$

The variance of the output is then

$$\sigma_y^2 = E\left[(y - Gd)(y - Gd)^H\right] = E\left[\mathbf{w}^H \mathbf{n}\mathbf{n}\mathbf{w}^H\right] = \mathbf{w}^H \mathbf{R}_{nn} \mathbf{w} \tag{2.15}$$

Using Lagrange method to solve equation 2.15 under the constraint that $\mathbf{w}^H\mathbf{c} - G = 0$, the quantity that needs to be minimized is

$$L = \mathbf{w}^H \mathbf{R}_{nn} \mathbf{w} - \lambda(\mathbf{w}^H \mathbf{c} - G)$$

This can be minimized by setting it's gradient, with respect to $\mathbf{w}^H$, to zero yielding

$$\nabla_w L = \mathbf{R}_{nn}\mathbf{w} - \lambda \mathbf{c} = 0$$
$$\mathbf{w} = \lambda \mathbf{R}_{nn}^{-1} \mathbf{c}$$

The constraint $\mathbf{w}^H\mathbf{c} = G$ means that $\lambda = \frac{G^*}{\mathbf{c}^H \mathbf{R}_{nn}^{-1} \mathbf{c}}$. It immediately follows that the weight vector resulting in the optimum LCMV solution is of the form

$$\mathbf{w}_{LCMV} = \beta_{LCMV} \mathbf{R}_{nn}^{-1} \mathbf{c} \tag{2.16}$$

where $\beta_{LCMV} = \lambda = \frac{G^*}{\mathbf{c}^H \mathbf{R}_{nn}^{-1} \mathbf{c}}$

2.3.3 Maximum Signal-to-Interference and Noise Ratio (MSINR)

Another performance criterion is maximization of the desired signal's SINR at the output of the OC combiner. Using equation 2.13, the average output SINR is

$$SINR = \sigma_s^2 \frac{\mathbf{w}^H \mathbf{c}(\mathbf{c})^H \mathbf{w}}{\mathbf{w}^H \mathbf{n}\mathbf{n}^H \mathbf{w}} \tag{2.17}$$

$$= \sigma_s^2 \frac{(\mathbf{w}^H \mathbf{c})^2}{\mathbf{w}^H \mathbf{R}_{nn} \mathbf{w}} \tag{2.18}$$

which can be rewritten as

$$SINR = \sigma_s^2 \frac{\left[(\mathbf{R}_{nn}^{1/2}\mathbf{w})^H (\mathbf{R}_{nn}^{-1/2}\mathbf{c})\right]^2}{(\mathbf{R}_{nn}^{1/2}\mathbf{w})^H (\mathbf{R}_{nn}^{1/2}\mathbf{w})} \tag{2.19}$$

Applying the Cauchy-Schwartz inequality to the numerator of equation 2.19 yields:

$$\left[(\mathbf{R}_{nn}^{1/2}\mathbf{w})^H (\mathbf{R}_{nn}^{-1/2}\mathbf{c})\right]^2 \leq \left[(\mathbf{R}_{nn}^{1/2}\mathbf{w})(\mathbf{R}_{nn}^{1/2}\mathbf{w})^H\right] \left[(\mathbf{R}_{nn}^{-1/2}\mathbf{c})(\mathbf{R}_{nn}^{-1/2}\mathbf{c})^H\right]$$

Therefore the upper bound of the OC SINR is

$$SINR \leq \sigma_s^2 \frac{\left[(\mathbf{R}_{nn}^{1/2}\mathbf{w})^H (\mathbf{R}_{nn}^{1/2}\mathbf{w})\right] \left[(\mathbf{R}_{nn}^{-1/2}\mathbf{c})^H (\mathbf{R}_{nn}^{-1/2}\mathbf{c})\right]}{(\mathbf{R}_{nn}^{1/2}\mathbf{w})^H (\mathbf{R}_{nn}^{1/2}\mathbf{w})} = \sigma_s^2 (\mathbf{R}_{nn}^{-1/2}\mathbf{c})^H (\mathbf{R}_{nn}^{-1/2}\mathbf{c})$$

Equality is guaranteed for the Cauchy-Schwartz inequality when the vectors $\mathbf{R}_{nn}^{1/2}\mathbf{w}$ and $\mathbf{R}_{nn}^{-1/2}\mathbf{c}$ are parallel, ie:

$$\mathbf{R}_{nn}^{1/2}\mathbf{w} = \alpha \mathbf{R}_{nn}^{-1/2}\mathbf{c} \tag{2.20}$$

or

$$\mathbf{w_{MSINR}} = \alpha \mathbf{R}_{nn}^{-1}\mathbf{c} \tag{2.21}$$

where α is a scalar factor which may be set to unity. The resultant maximized SINR is

$$SINR = \sigma_s^2 \mathbf{c}^H \mathbf{R}_{nn}^{-1}\mathbf{c} \tag{2.22}$$

2.3.4 Maximum Likelihood (ML)

With the maximum likelihood performance criterion, the desired signal is considered deterministic but unknown and it's estimation is the goal. The received signal is given as in equation 2.6 and the maximum likelihood estimate of d, the desired signal, denoted by $\hat{d}$ is the value of s which maximizes the probability function $f_{\mathbf{x}|s}(\mathbf{x}|s)$

Assuming that $\mathbf{n}$ has a zero mean Gaussian distribution then, $f_{\mathbf{x}|s}(\mathbf{x}|s)$ is a multivariate Gaussian distribution with mean $\mathbf{c}s$ and coveriance matrix $\mathbf{R}_{nn}$

If we assume that $\mathbf{x}$, the digitized continuous signal $\mathbf{x(t)}$, has length N, then the multivariate probability density function of $\mathbf{x}$ is

$$f_{\mathbf{x}|s}(\mathbf{x}|s) = \frac{1}{\pi^N |\mathbf{R}_{nn}|} e^{-(\mathbf{x}-\mathbf{c}s)\mathbf{R}_{nn}^{-1}(\mathbf{x}-\mathbf{c}s)^H}$$

Our objective is to maximize $f_{\mathbf{x}|s}(\mathbf{x}|s)$. This is equivalent to maximizing

$$LLR(\mathbf{x}|s) = ln\left(\frac{1}{\pi^N |\mathbf{R}_{nn}|} - (\mathbf{x}-\mathbf{c}s)\mathbf{R}_{nn}^{-1}(\mathbf{x}-\mathbf{c}s)^H\right)$$

Setting the partial derivative of $LLR(\mathbf{x}|s)$ with respect to s^* equal to zero and solving

for s, gives

$$\hat{s} = \frac{\mathbf{c}^H \mathbf{R}_{nn}^{-1}}{\mathbf{c}^H \mathbf{R}_{nn}^{-1} \mathbf{c}} \mathbf{x}$$

Hence, the maximum likelihood array output is of the form

$$y = \hat{s} = \mathbf{w}_{ML}^H \mathbf{x}$$

where

$$\mathbf{w}_{ML}^H = \beta_{ML} \mathbf{R}_{nn}^{-1} \mathbf{c} \tag{2.23}$$

$$\beta_{ML} = \frac{1}{\mathbf{c}^H \mathbf{R}_{nn}^{-1} \mathbf{c}}$$

It is worth noting that the ML solution is identical to the LCMV solution when the LCMV output is constrained to be an unbiased estimate of the desired signal, ie: $G = 1$.

2.4 SINR Dependence on Cross Correlation Properties of Propagation Environment

In this section, SINR dependence on cross correlation properties of the propagation environment is explored. Henceforth, the general multi-antenna view point is dropped in favor of a dual antenna approach, since analysis of dual antenna systems is simpler than that of general multi-antenna systems. The first part of this section presents the power (ρ_p), envelope (ρ_e), and complex signal (ρ_s) cross correlation coefficients for a dual antenna system; the second part explores how the performance of MRC and OC depends on the cross correlation coefficients

The signal power correlation coefficient is expressed as

$$\rho_p = \frac{E[P_1 P_2]}{E[P_1 P_1] E[P_2 P_2]} \tag{2.24}$$

where P_1 and P_2 are the zero mean signal powers.

The signal envelope correlation coefficient is defined as

$$\rho_e = \frac{E[e_1 e_2]}{E[e_1 e_1] E[e_2 e_2]} \tag{2.25}$$

where e_1 and e_2 are the zero mean absolute values of the complex baseband voltages of the received signal.

The complex signal correlation coefficient may be defined as

$$\rho_s = \frac{E[s_1 s_2]}{E[s_1 s_1] E[s_2 s_2]} \tag{2.26}$$

where s_1 and s_2 are the zero mean complex baseband voltages.

Of the three correlation coefficeints envelope correlation coefficient is most commonly reference in literature. Although envelope correlation is often used to indicate how

much SINR gains is obtainable from diversity antenna systems, those gains are dependent on the combining scheme used. The envelope correlation coefficient alone is an insufficient indication of the performance of OC; envelope correlation coefficient does not contain information about the relative phase of complex baseband signals at the two diversity antennas (see subsection 2.4.2. Nevertheless, it has been shown that $\rho_e \approx \rho_p$ and that in Rayleigh fading environments $|\rho_s|^2 \approx \rho_e$ [5].

The power and envelope correlation coefficients are an indication of the probability of a multi-path multipath fade at one antenna occurring at the same time as a fade at another antenna. In a real system, signal fading is due to both short term and long term fading. Short term (multi-path) fading is caused by destructive combining of multi-path components. Long term fading is caused by differences observed in the environment as the mobile travels a distance of several wavelengths. In order to obtain a meaningful estimate of the cross correlation long term fading component of the received signal are removed.

The complex baseband voltages, signal envelopes and signal power can be normalized in the same manner. Normalization of the envelope correlation is accomplished by assuming that the received signal envelope, $r(t)$, is a product of a slow (low frequency) moving average, $m(t)$, due to long term fading, and a faster varying (high frequency) term, $e'(t)$, due to short term fading.

$$r(t) = e'(t)m(t) \tag{2.27}$$

The moving average over a window of length 2L is given by:

$$m(t) = \frac{1}{2L}\int_{t-L}^{t+L} r(\tau)d\tau \tag{2.28}$$

The normalized zero mean signal envelope is then given by

$$e(t) = e'(t) - 1 = \frac{r(t)}{m(t)} - 1 \tag{2.29}$$

Proper selection of the window size $2L$ is important. Using the local mean to remove the long term fading component out of the received signal envelope is synonymous to trying to remove the low frequency component out of a signal using a high pass filter (HPF) where $\frac{1}{2L}$ is proportional to the cutoff frequency of the HPF. If the length $2L$ of the local mean estimate is too large, the HPF will be insufficient to remove all but the slowest varying components due to long term fading; if the length is too small then the HPF filter will also remove some components due to short term fading. Typical measurement lengths of the local mean correspond to a mobile traveling a distance of 5 to 20 wavelengths.

In litterature, lower cross correlation coefficient is said to indicate higher SINR gains. This is true for SD, EGC, and MRC. However, the OC SINR gain may still increase in the presence of high cross correlation coefficient. In this thesis, therefore, the cross correlation coefficients are not used to estimate SINR gains. Approximate SINR gains are provided and used to provide insite into the cross correlation properties of the propagation environment. Although it would have been insightfull to observe the distribution of ρ_s and $|\rho_s|^2$, the digitization process used in logging the RF signals prevented this. (See section 4.2.3)

The SINR gain of any dual antenna system is comprised of diversity gain and combining gain. Diversity gain (DG) is derived from the simple fact that there is more than one receive antenna. Multi-path fading at one antenna does not necessarily coincide with multi-path fading at the other and the dual input receiver can selectively choose to receive from the better of the two antennas. Combining gain is derived from the combining scheme. The combining gain (CG) is a measure of the combining scheme's ability to intelligently combine received signals so that the desired signal power is increased while noise and interference power are reduced. In this report the metric

used to evaluate the performance of SD, MRC and OC combining schemes is the total SINR gain although relationships exist between SINR gain, DG, and CG

$$SINR(dB) = 10log_{10}SINR_{CombiningScheme} - 10log_{10}SINR_{strongest-antenna},$$
$$DG(dB) = 10log_{10}SINR_{SD} - 10log_{10}SINR_{strongest-antenna},$$
$$CG(dB) = 10log_{10}SINR_{CombiningScheme} - 10log_{10}SINR_{SD}$$

MRC and OC are complicated combining methods. They require more complex hardware than SD because of use of complex weighting and combining. MRC and OC are therefore viable combining schemes when $SINR_{MRC} \geq SINR_{SD}$ and $SINR_{OC} \geq SINR_{SD}$ respectively.

Assuming that the received signal at the dual antenna ports are of the form

$$\begin{bmatrix} x_1 \\ x_2 \end{bmatrix} = \begin{bmatrix} c_1 \\ c_2 \end{bmatrix} s + \begin{bmatrix} n_1 \\ n_2 \end{bmatrix} \tag{2.30}$$

Where s is the desired transmitted signal, c_i and n_i are respectively the complex fading coefficient and noise plus interference at antenna i.

The SINR of the desired signal at antenna i before combining is

$$SINR_i = \frac{\sigma_s^2}{\sigma_{n,i}^2}\left(|c_i|^2\right) \tag{2.31}$$

The output signal at the combiner filter output is

$$y = \begin{bmatrix} w_1^* & w_2^* \end{bmatrix} \begin{bmatrix} x_1 \\ x_2 \end{bmatrix} = \begin{bmatrix} w_1^* & w_2^* \end{bmatrix} \begin{bmatrix} c_1 \\ c_2 \end{bmatrix} s + \begin{bmatrix} w_1^* & w_2^* \end{bmatrix} \begin{bmatrix} n_1 \\ n_2 \end{bmatrix} \tag{2.32}$$

2.4.1 Maximum Ratio Combining (MRC)

The MRC combiner chooses the weight vector as

$$\mathbf{w} = \begin{bmatrix} \frac{c_1}{\sigma_{n,1}^2} \\ \frac{c_2}{\sigma_{n,2}^2} \end{bmatrix}$$

The output signal at the MRC combiner output is therefore

$$y = (\frac{|c_1|^2}{\sigma_{n,1}^2} + \frac{|c_2|^2}{\sigma_{n,2}^2})s + \frac{c_1 n_1}{\sigma_{n,1}^2} + \frac{c_2 n_2}{\sigma_{n,2}^2}$$

Using a little algebra the SINR at the MRC filter output can be found as

$$SINR_{MRC} = \frac{\sigma_s^2 \left(\frac{|c_1|^2}{\sigma_{n,1}^2} + \frac{|c_2|^2}{\sigma_{n,2}^2}\right)^2}{\frac{|c_1|^2}{\sigma_{n,1}^2} + \frac{|c_2|^2}{\sigma_{n,2}^2} + \frac{E[n_1 n_2]c_1 c_2^*}{\sigma_{n,1}^2 \sigma_{n,2}^2} + \frac{E[n_2 n_1]c_2 c_1^*}{\sigma_{n,1}^2 \sigma_{n,2}^2}} \tag{2.33}$$

If we defined $\rho_s(s) = \frac{c_1 c_2^*}{|c_1||c_2|}$ as the complex cross correlation of the desired signal at the two received antennas, make the substitution $SINR_1 = \frac{\sigma_s^2 |c_1|^2}{\sigma_{n,1^2}}$, and assume that $SINR_1 \geq SINR_2$ then equation 2.33 is transformable to

$$SINR_{MRC} = SINR_1 \left(\frac{\left(1 + \frac{SINR_2}{SINR_1}\right)^2}{1 + \frac{SINR_2}{SINR_1} + 2\sqrt{\frac{SINR_2}{SINR_1}} R\left[\rho_s(s)\rho_s^*(n)\right]} \right) \tag{2.34}$$

$$SINRgain_{MRC}(dB) = 10log_{10} \left(\frac{SINR_1}{SINR_2} \frac{1 + \frac{SINR_2}{SINR_1}}{1 + \sqrt{\frac{SINR_2}{SINR_1}} \frac{2R[\rho_s(s)\rho_s^*(n)]}{1 + \frac{SINR_2}{SINR_1}}} \right) \tag{2.35}$$

Thus when the noise plus interference is white, the SINR gain when using MRC is always guaranteed to be greater than 0dB; it is 3 dB when SINR at the two antenna ter-

minals are equal. When the cross correlation of noise plus interference increases above zero, the noise plus interference power increases by a factor of $\sqrt{\frac{SINR_2}{SINR_1}}\Re\left[\rho_s(s)\rho_s^*(n)\right]$. The SINR gain therefore decreases with an increase in the cross correlation of noise plus interference. For very closely spaced antenna elements it can be expected that $\rho_s(n) \neq 0, \rho_s(s) \neq 0$ so that noise plus interference power amplification reduces the MRC SINR gains.

2.4.2 Optimum Combining (OC)

The OC combiner chooses the weight vector as

$$\mathbf{w} = \mathbf{R}_{nn}^{-1}\mathbf{c} = \begin{bmatrix} \sigma_{n,1}^2 & E\left[n_1 n_2\right] \\ E\left[n_2 n_1\right] & \sigma_{n,2}^2 \end{bmatrix}^{-1} = \frac{1}{\sigma_{n,1}\sigma_{n,2}\left(1-|\rho_s(2)|^2\right)} \begin{bmatrix} \frac{\sigma_{n,2}}{\sigma_{n,1}} & -\rho_s(n) \\ -\rho_s^*(n) & \frac{\sigma_{n,1}}{\sigma_{n,2}} \end{bmatrix} \begin{bmatrix} c_1 \\ c_2 \end{bmatrix} \tag{2.36}$$

The output of the OC filter is

$$\begin{aligned} y = \mathbf{w}^H\mathbf{x} &= \begin{bmatrix} c_1^* & c_2^* \end{bmatrix} \frac{1}{\sigma_{n,1}\sigma_{n,2}\left(1-|\rho_s(n)|^2\right)} \begin{bmatrix} \frac{\sigma_{n,2}}{\sigma_{n,1}} & -\rho_s(n) \\ -\rho_s^*(n) & \frac{\sigma_{n,1}}{\sigma_{n,2}} \end{bmatrix} \begin{bmatrix} x_1 \\ x_2 \end{bmatrix} \\ &= \begin{bmatrix} c_1^* & c_2^* \end{bmatrix} \frac{1}{\sigma_{n,1}\sigma_{n,2}\left(1-|\rho_s(n)|^2\right)} \begin{bmatrix} \frac{\sigma_{n,2}}{\sigma_{n,1}}x_1 - \rho_s(n)x_2 \\ \frac{\sigma_{n,1}}{\sigma_{n,2}}x_2 - \rho_s^*(n)x_1 \end{bmatrix} \end{aligned} \tag{2.37}$$

It can be seen from the expression above that the $\mathbf{R}_{nn}^{-1}$ matrix component of $\mathbf{w}$ acts to normalize, co-phase and cancel the correlated components of noise plus interference from the received signal on both antennas. This leaves the noise plus interference component that is non-correlated at the two receive antennas. Components of the desired signal which are correlated to the noise plus interference at the two antennas are also reduced. The $\mathbf{c}$ component of $\mathbf{w}$ then co-phases the residual desired signal components and adds them in the presence of the residual non-correlated noise plus interference. In signal processing terms, the total received signal is first passed

through a pre-whitening filter the output of which is then passed through an EGC combiner.

The resultant output SINR is

$$\begin{aligned}
SINR_{OC} &= \sigma_s^2 \mathbf{c}^H \mathbf{R}_{nn}^{-1} \mathbf{c} \\
&= \sigma_s^2 \begin{bmatrix} c_1^* & c_2^* \end{bmatrix} \frac{1}{\sigma_{n,1}\sigma_{n,2}\left(1-|\rho_s(n)|^2\right)} \begin{bmatrix} \frac{\sigma_{n,2}}{\sigma_{n,1}} & -\rho_s(n) \\ -\rho_s^*(n) & \frac{\sigma_{n,1}}{\sigma_{n,2}} \end{bmatrix} \begin{bmatrix} c_1 \\ c_2 \end{bmatrix} \\
&= \frac{\sigma_s^2}{\sigma_{n,1}\sigma_{n,2}\left(1-|\rho_s(n)|^2\right)} \left(|c_1|^2 \frac{\sigma_{n,2}}{\sigma_{n,1}} + |c_2|^2 \frac{\sigma_{n,1}}{\sigma_{n,2}} - (\rho_s^*(n) c_1 c_2^* + \rho_s(n) c_1^* c_2) \right) \\
&= \frac{\sigma_s^2 |c_1|^2}{\sigma_{n,1}^2} \frac{1 + \frac{SINR_2}{SINR_1} - 2\left(\sqrt{\frac{SINR_2}{SINR_1}}\right) R\left[\rho_s(s)\rho_s^*(n)\right]}{1-|\rho_s(n)|^2} \\
&= SINR_1 \frac{1 + \frac{SINR_2}{SINR_1} - 2\left(\sqrt{\frac{SINR_2}{SINR_1}}\right) R\left[\rho_s(s)\rho_s^*(n)\right]}{1-|\rho_s(n)|^2}
\end{aligned} \tag{2.38}$$

and the SINR gain is

$$SINRgain_{OC}(dB) = 10log_{10}\left(\frac{1 + \frac{SINR_1}{SINR_2} - 2\left(\sqrt{\frac{SINR_1}{SINR_2}}\right) R\left[\rho_s(s)\rho_s^*(n)\right]}{1-|\rho_s(n)|^2} \right) \tag{2.39}$$

When the complex cross correlation of the noise plus interference signals at the two antennas is zero, the OC SINR gain is guaranteed to exceed 0dB and is 3dB when the SINR at the two antennas are equal. When the cross correlation of noise plus interference, $\rho_s(n)$, increases above zero, the received signal power is reduced by a factor of $2\left(\sqrt{\frac{SINR_2}{SINR_1}}\right) R\left[\rho_s(s)\rho_s^*(n)\right]$. This causes a partial decrease in the SINR gain because of signal cancellation. At the same time, an increase in $\rho_s(n)$ decreases the noise plus interference power by a factor of $|\rho_s(n)|^2$ and thereby partially increases the SINR gain. With OC, an increase in $\rho_s(n)$ increases the SINR gain if the reduction in interference and noise power more than compensates for the reduction in desired signal power due to signal cancellation.

Chapter 3

IS-95 Forward Link Physical Layer

The purpose of this chapter is to present the IS-95 Forward Link Physical layer. A brief technical overview of the IS-95 Forward Link Physical layer is given as background for the measurement procedures and data process undertaken. Forward Link Transmitter and Receiver are discussed. The reader who is familiar with IS-95 may wish to skip this chapter.

3.1 Brief Technical Overview

The IS-95 standard details the requirements for analog and digital operation of mobile and base stations that employ Code Division Multiple Access (CDMA). This report focuses on the digital aspects of IS-95, and although an attempt is made to cover all pertinent components of IS-95 Forward Link Physical Layer the reader is referred to [1] for a more complete description.

The multiple-access scheme employed in IS-95 is CDMA. All base stations in a CDMA network operate using the same carrier frequency. Spreading codes are used to separate signals. Each user's signal is spread with a 1.2288 Mega chips per second (Mcps) spreading sequence. In a communications channel with only a single path, the spreading sequence ensures that the transmitted signals of one base station sector

is orthogonal to that of every other sector. Typical wireless radio propagation channels are however multi-path. Multi-path leads to fading of the received signal and a breakdown in the orthogonality of the spread sequences. The loss of orthogonality leads to co-channel interference from signals transmitted from other base station sectors that share the same CDMA frequency band.

The performance and capacity of an IS-95 network is limited by multi-path fading and the co-channel interference each mobile station experiences from sectors on the same network other than the one serving the mobile station . IS-95 has many mechanisms designed to mitigate multi-path fading and co-channel Interference. System performance is improved by the use of macro-diversity and rake reception. Interference is reduced using a variable viterbi vocoder and power control. With macro-diversity multiple base stations transmit the same signal to a subscriber. This improves signal reception by allowing the subscriber to be in soft handoff. With rake reception multiple time delayed versions of the signal transmitted by a particular base station are combined to improves signal reception. The use of a variable vocoder reduces the overall interference in the system because it lowers the transmitted bit rate during quiet periods; and power control forces all base station sectors to carefully regulate the power transmitted and thereby reduces interference seen by mobile stations it is not servicing.

Although macro-diversity, rake reception, variable rate vocoder, and power control reduce multi-path fading and co-channel interference; and increase the perceived SINR, multi-path fading and co-channel interference are not completely eliminated. The inclusion of diversity antennas at the mobile station promises to further increase the SINR on the Forward Link. In particular such a mechanism is required on the forward link to reduce the interference power at the mobile station. This may be done using two diversity antennas on the mobile station and an algorithm to reduce interference and noise power while maximizing the desired signal power.

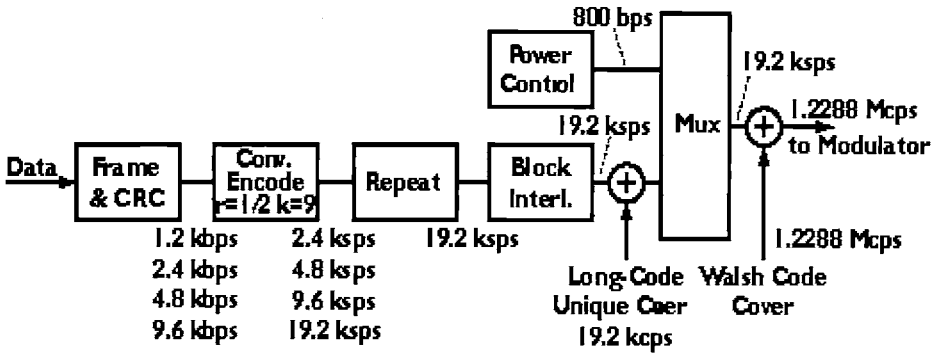

Figure 3-1: Forward link processing

3.2 IS-95 Forward Link Transmitter

For the measurements reported in this report, signals were logged from SPRINT PCS's IS-95 compatible network. An understanding of the IS-95 forward link transmitter is presented to provide the background for the methods used to detect the CDMA signals. The mechanism employed to emulate the forward link receiver structure (that de-spreads the CDMA signals) is complementary to the mechanisms used to spread signals transmitted on the the forward link.

3.2.1 Channelization

The forward link consists of up to 64 logical (code) channels. The channels are independent in that they carry different data streams, at possibly different data rates, and are independently adjustable in amplitude. The channels are a single pilot channel, and a number of sync, paging, and traffic channels.

3.2.2 Coding and interleaving

Figure 3-1 shows the core processing that generates one forward code channel, at rate set 1. Rate set 2 is identical except the coding rate is 3/4 rather than 1/2 yielding the same code rate with 3/2 times the data rate.

3.2.3 Walsh Codes

The code channels as transmitted, are mathematically orthogonal. Orthogonality is established by covering the coded symbols out of the MUX in figure 3-1 with one of a set of 64 mutually orthogonal Walsh functions. "Mutually orthogonal" means that the cross correlations of any two Walsh functions are small (ideally zero). Since only whole periods of the Walsh functions occur in each code symbol, the effect of the Walsh cover is to make the channels completely separable in the receiver in the absence of multi-path. The orthogonality not only means that there is no co-mingling of channels, it means there is no interference between users in the same cell, again in the absence of multi-path. This has a substantial beneficial effect on the forward link capacity.

Multi-path delay spread that exceeds a chip duration introduces mutual interference between users in a cell. The interference level is zero when there is only one multi-path component and increases with the number of multi-path components.

One of the Walsh functions is always a constant, code number zero, by the numbering convention. This channel is always reserved to serve as the Pilot Channel.

3.2.4 Spreading

Each forward code channel is spread by the Short Code, which has I- and Q-components. The spreading is thus quadrature. That is, from a single binary-valued, covered, symbol stream, two binary sequences are generated by mod 2 addition of the short code PN sequences, as shown in figure 3-2.

3.2.5 Forward Link Channels

Other than the traffic channels there are three types of channels in the forward link: pilot, sync, and paging. The pilot is required in every base station.

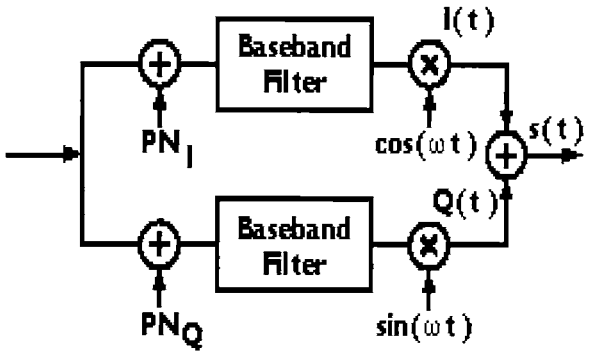

Figure 3-2: Quadrature spreading

Pilot Channel

The pilot channel is always code channel zero (Walsh function zero). It is both a demodulation reference for the mobile receivers, and for handoff level measurements; it is, therefore, present in every base station. It carries no information bits but is pure PN short code, with no additional cover or information content.

The amplitude of the pilot and its spatial distribution are carefully controlled. The PNI and PNQ modified linear feedback shift register sequences that comprise the short code have period 2^{15} chips, which is 26.667 ms at the 1.2288 Mcps chip rate.

All stations use the same short code, and thus have the same pilot waveform. They are distinguished from one another only by the phase of the pilot. The phase of the pilot is related to it's delay from the start of CDMA time modulo 2^{15}. This delay in chips is called the pilot's PN offset. The period of the short code, 2^{15}, facilitates rapid pilot searches by the mobiles.

The air interfaces stipulate that pilot phases always be assigned to stations in multiples of 64 chips, giving a total of $2^{15-6} = 512$ possible assignments. The 9-bit number that identifies the pilot phase assignment is called the pilot offset.

Sync, Paging and Traffic Channels

The sync channel carries a repeating message that identifies the station, and the absolute phase of the pilot sequence. The sync channel is covered using Walsh Function 32. The paging channel conveys pages, which are notifications of incoming calls, to the mobile stations. Traffic channels confers voice and data to and from the mobile station during call processing. The Sync Channel is covered using Walsh Function 32, and the Paging and Traffic Channels are covered using the remaining 62 Walsh functions and masked using the Long PN sequence. Each of the Paging and Traffic channels is then masked using the same Long PN sequence but with different delay. The Long PN sequence is similar to the Short PN Sequence except that it is 2^{41} chips long. Knowledge of the particular Long PN Sequence delay is required to demodulate the Paging and Traffic Channels.

3.2.6 Timing

All base stations must be synchronized within a few microseconds for the station identification mechanisms to work reliably and without ambiguity. The system was designed under the assumption that the Global Positioning System (GPS) would be used. This is a family of low-earth-orbit satellites that broadcast a spread-spectrum signal and ephemeris information from which a sophisticated Kalman filter algorithm in a receiver can derive both a very accurate position and a very accurate time. Timing in IS-95 systems is by CDMA time which is derived from GPS time.

Chapter 4

Measurement System

4.1 Experimental Setup and Procedure

The transmitters for the measurements were standard IS-95 CDMA base stations belonging to the SPRINT PCS network in San Diego. These base stations were transmitting at 19231.25 MHz; they were publicly deployed and servicing SPRINT PCS's customers. The exact number and location of the base stations were unknown.

On the receive end, a mobile handset equipped with a top mounted monopole and an internal monopole mounted at the back of the handset, was employed (figure 4-1). The top mounted monopole was labeled Antenna 1 and the internal monopole antenna is Antenna 2. The top-mounted monopole and internal monopole impedances were also measured to ensure that they matched. RF cables of the same length were used in connecting the dipole antennas to the logging device; the impedance of the cables was measured to ensure that the antennas still matched when connected to the measuring device via the RF cables.

A measurement van was used to hold all the test equipment as well as to mimic the typical vehicle borne, mobile user. Measurements were taken with the van moving at normal traffic speeds: ranging from 15MPH to 40MPH with intermittent stops depending on traffic situations. The dimensions of the test van and its interior might

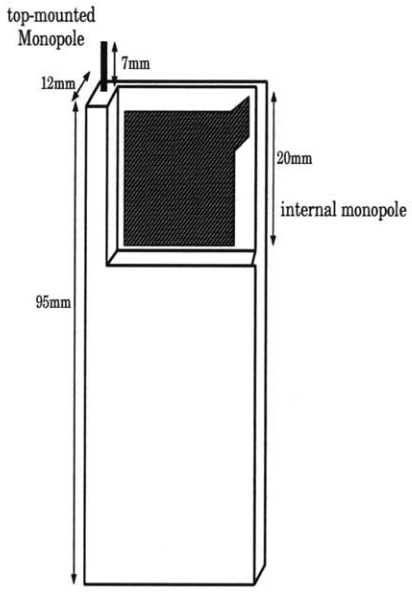

Figure 4-1: Mobile handset with top mounted monopole and patch antenna at back

Figure 4-2: Measurement van with phantom head dummy

be of importance for environment characterization. Figure 4-2 shows the details of the interior of the van. When the mobile handset is placed next to the window, the signals it receives face diffraction by the front windshield, and obstruction by the van's interior panels and the phantom head. When the mobile is facing the inside of the van, the signals it received were diffracted by the windshield and obstructed by the person driving the van as well as other objects in the interior of the van.

The effect of an operator's hand on the performance of the combining schemes was tested by performing repeated trials using a phantom head dummy and an actual human operator. A phantom head dummy was used to simulate the effects of head blockage on the signal reception and the combining schemes. The phantom head

dummy was filled with electrolyte with the same electrical absorption characteristics as the typical human head. When in use, the phantom head was placed at the front passenger seat of the measurement van and the mobile handset was placed at the side of the phantom head dummy next to the window or facing the inside of the van. At other times a person held the mobile handset next to his ear, partially covering a section of the internal monopole with his hand. This configuration was meant to test the effects of hand blockage on the signal reception capabilities of the diversity antenna mobile handset.

For each test, signals impinging on the two diversity antennas were logged simultaneously. Data was taken with the the mobile handset inside the van and while the measurement van was moving at about 15 to 40 miles per hour with intermittent stops and turns as dictated by traffic conditions. Drive tests were taken in three areas: open area where few one-story buildings provide little local scattering; in the residential area where many clustered, one-story homes provide mild local scattering; and in the downtown area where closely packed, high rise buildings provide severe local scattering around the mobile. The open area drive route starts from the intersection of Mirimar Road and Kearny Villa Road and ends on Mirimar Road; the residential area drive route is a five minute long route in the Mira Mesa residential area; and the downtown area is a five minute route around the Horton Plaza starting on 4th Avenue and ending on Broadway Street. (See figure 4-3).

Measurements were taken by digitizing and recording of the RF voltages of 2 antennas with 5 MHz instantaneous bandwidth. Both channels were logged simultaneously and synchronized in both time and RF phase. Implementation of the combining schemes, and analysis of the results were done using Matlab.

The propagation channel varies with time because of Doppler shift. The methods for computing MRC and OC weights require the assumption of a static channel during data taking. The propagation environment was sampled using a sampling duration of $0.0017s$, which allowed the static channel assumption to hold for moderate Doppler Shifts.

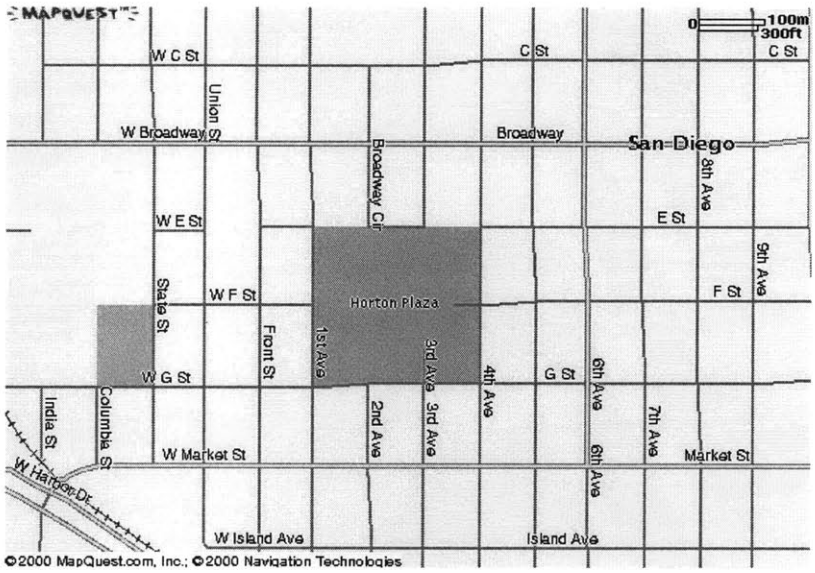

Figure 4-3: Downtown area

Voltages corresponding to CDMA signals at 1931.25 MHz center frequency were logged from the SPRINT PCS system. The logged voltages were processed to yield channel path gains for detected pilot signals. Figure 4-4 illustrates the process used to generate and apply the MRC and OC weights after the signals were digitized at 5MHz. The digitized signals were corrected for a rolling error in the sampling clock, down-sampled to 1.2288 Mega Samples per second (MSps) (Chipx1), and de-spread using standard PN sequences. Then the complex fading coefficients of the detected pilot signals were used to approximate MRC and OC weights. The weights are applied to the digitized signals at each antenna and the weighted signals added. The combined signal was again de-spread using standard PN sequences. A desired signal whose SINR was to be maximized was selected. Cumulative Distribution Function (CDF) plots of the SINR of the desired signal at the output of the SD, MRC and OC combiner were generated and compared to the cumulative distribution plots of the two diversity antennas; this gave the diversity gain of using SD and the SINR gains of MRC and OC.

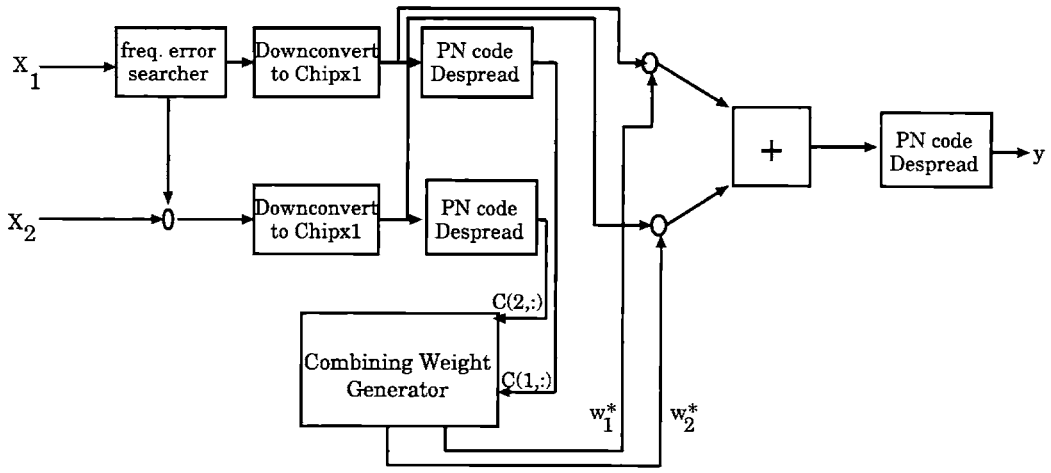

Figure 4-4: Weight generation and application block

4.2 Parameter Estimation

Voltages corresponding to CDMA signals at 1931.25 MHz center frequency were logged from the SPRINT PCS system. Logging CDMA signals from a commercially deployed cellular system allows the SINR gains reported in this paper to be free from simplifications and assumptions used in models and simulations. This section describes how the logged voltages were processed to yield channel path gains.

The general scheme used to extract channel parameters is shown in figure 4-5. The received RF waveform is down-sampled to 70 MHz and then digitized at 5 Mega samples per second (MS/s). The down-sampled samples are then correlated against the standard IS-95 PN Sequence to yield pilot weighted complex path gains for each PN offset.

The following analysis of parameter estimation is an extention of work by Micheal Wengler of Qualcomm Inc. on the measuring device. Because that documentation is not publicly available, the analysis is repeated here. Additions to Micheal Wengler's work include explanations of how the frequency error of the sampling clock is corrected.

4.2.1 Signal Model

Radiated Signal

Let $I(t)$ and $Q(t)$ be the in-phase and quadrature-phase pseudo-random-noise (PN) sequences in the IS-95 standard. $I(t)$ and $Q(t)$ take on values in the set $\{-1, +1\}$ for a chip duration. Let $\tau_s = \frac{1}{1228800} s$ represent the chip duration. Let $LONGCODEMASK_w$ be the long PN sequence used to mask the paging or traffic channel indexed by w, and D_w be one of the Walsh codes used for channelization on the forwards link such that D_0 specifies the Pilot Channel and is the all '0's signal; n enumerates a particular radiating sector of a CDMA cellular system and $s(t)$ represent the complex baseband pilot having no time delay and band-limited to 625kHz. ie,:

$$s(t) = (I(t) - jQ(t))) \left(D_0 + \sum_{w=1}^{63} D_w LONGCODEMASK_w \right) \tag{4.1}$$

Let $\tau_n = PNOFFSET_n * \tau_c$ be the PN offset used to define a particular sector n. Then the complex baseband pilot signal radiating from sector n is given by

$$s_n = s(t - \tau_n) \tag{4.2}$$

Each sector pilot therefore radiates $\Re\{s_n e^{(j\omega t)}\}$.

RF Propagation Channel

The channel that the signal propagates through includes varying path gain, time delay between the sector n and the receive antenna, and coupling to the antennas at the mobile. Path loss leads to signal components being lower in magnitude. Multiple paths for the signal components means that the received signal is a sum of components from sector n to receiver m along path i where $(1 < i \leq L)$. Consider a mobile handset

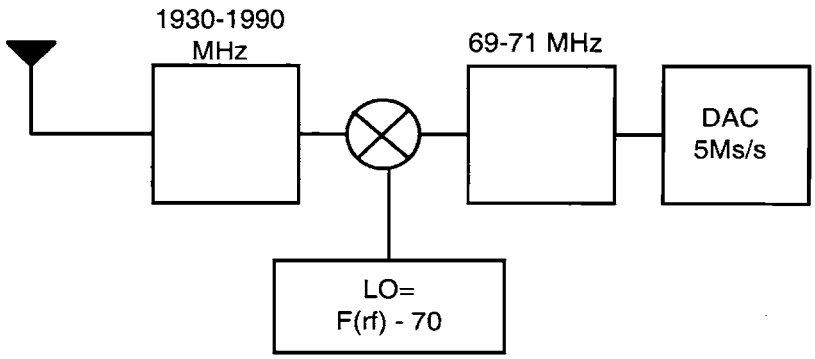

Figure 4-5: System used to down-sample, digitize and log RF signals

with M diversity antennas. The received voltage at antenna m is

$$r_m = \Re\left[n_m(t) + \sum_n \sum_i \beta_{i,n,m} e^{(j\omega(t-t_{i,n,m}))} s_n(t - t_{i,n,m})\right] \tag{4.3}$$

where $\beta_{i,n,m}$ and $t_{i,n,m}$ are respectively the amplitude of the path gain, and the time delay along the ith path from sector n to antenna m on the received mobile handset. $n_m(t)$ is the noise in the system and co-channel interference in the system.

The time delay $t_{i,n,m}$ causes the phase of the signal components to change by a fixed phase. Let that path dependent phase offset be

$$\theta_{i,n,m} = mod\,(\omega t_{i,n,m}, 2\pi) \tag{4.4}$$

The received voltage at antenna m may be re-written in terms of the path gain (amplitude) and fixed phase as

$$r_m = \Re\{n_m(t) + \sum_n \sum_i \beta_{i,n,m} e^{(j\omega(t-\theta_{i,n,m}))} s_n(t - t_{i,n,m})\} \tag{4.5}$$

4.2.2 Channel Estimation

Figure 4-5 shows the system used to down-sample, digitize, and log the RF signals. The 1931.25MHz signal is mixed down to 70MHz, passed though a 70 +/- 1 MHz

filter and sampled using a $(5 + / - \delta f)$ MSps A2DC where $-0.00018MHz \leq \delta f \leq 0.00018MHz$ is the uncontrollable fluctuation in the sampling clock of the A2DC. The output voltage at the output of the ADC is

$$v_{m,k} = \Re \left[n_m(t) + \sum_n \sum_i \beta_{i,n,m} e^{j2/pi(14+\frac{14k\delta f}{5+\delta f}+1j\theta_{i,n,m})} \right] \tag{4.6}$$

and can be rewritten as

$$v_{m,k} = \Re \left[n_m(t_k) + \sum_n \sum_i \beta_{i,n,m} e^{(1j(\omega_e k+\theta_{i,n,m}))} s_n(t_k - t_{i,n,m}) \right] \tag{4.7}$$

where $t_k \approx \frac{k}{5*10^6}$ is the sampling time and $\omega_e = \frac{2\pi*14\delta f}{5+\delta f}$ is the frequency error after down-sampling and digitizing the received signal. A frequency searcher is applied to the digital samples $v_{m,k}$ to find the frequency error ω_e. The real voltage is then multiplied by $e^{-j\omega_e}$ to undo the effects of the frequency error. The result is re-sampled to 1228800 MS/s (Chipx1) and correlated with the standard PN sequence having a delay t_{probe}. This yields:

$$E\left(c'_{n,m}\right) = E\left[v_{m,k} e^{(j\omega_e k)} \left(I(k - t_{probe}) - jQ(k - t_{probe})\right)\right] \tag{4.8}$$

After substituting $s_k = I(k) - jQ(k)$ into the above equation and ignoring the $I(k) *$

$Q(k)$ product terms yields

$$
\begin{aligned}
E\{c_{n,m}\} =& E\{\Re\{n_m\}\} + E\{\sum_n \sum_i \beta_{i,n,m} \left(D_0 + \sum_w D_w LONGCODEMASK_w \right) * \\
& \{\cos(\omega_e k + \theta_{i,n,m}) \cos(\omega_e k) I(k - \tau_n - t_{i,n,m}) I(k - t_{probe}) \\
& + \sin(\omega_e k + \theta_{i,n,m}) \sin(\omega_e k) Q(k - \tau_n - t_{i,n,m}) Q(k - t_{probe}) \\
& - \cos(\omega_e k + \theta_{i,n,m}) \sin(\omega_e k) I(k - \tau_n - t_{i,n,m}) I(k - t_{probe}) \\
& + \sin(\omega_e k + \theta_{i,n,m}) \cos(\omega_e k) Q(k - \tau_n - t_{i,n,m}) Q(k - t_{probe})\}\}
\end{aligned}
\tag{4.9}
$$

For all i such that $t_{probe} - \tau_n - t_{i,n,m} \leq \tau_c$ (ie. For all multi-path components having PN sequence offsets within one chip duration of PROBE), the above terms reduce to

$$
E\left(c'_{n,m}\right) = E\left[D_0\right] \sum_i \beta_{i,n,m} e^{(j\theta_{i,n,m})} \tag{4.10}
$$

As PROBE moves through all 2^{15} possible PNoffsets the complex path gain from all detectable and resolvable sector pilot channels are obtained. From now on we use $a_{n,m} = E\left(c'_{n,m}\right) = E\left[D_0\right] \sum_i \beta_{i,n,m} e^{(j\theta_{i,n,m})}$ to represent the product of pilot signal strength from sector n at antenna m and the sum of the complex path gains from sector n to the antenna m for which the detected multi-path PNoffsets have path differences less than a chip duration. The sum over i includes all paths from sector n to antenna m whose delay differ by less than a chip duration. $a_{n,m}$ is proportional to the path gain and is referred to as pilot-weighted path gain.

The method used to perform channel parameter estimation is limited to a Chipx1 resolution. Multi-paths whose path lengths differ by less than a chip duration are not resolved. They are lumped together as a single pilot signal detection.

4.2.3 Estimation of MRC weight vector

The previous section explained how the product of the pilot-weighted path gain, $\mathbf{a}_{n,m}$, of the pilot signal from sector n to antenna m are obtained from the total received IS-95 CDMA signals logged from the SPRINT PCS network in San Diego.

Multi-path fading means that N pilot signals sent from N sectors yield $N_r > N$ detected pilot signals at and hence greater than N pilot-weighted path gains. The desired received signal needs to be chosen out of these N_r pilot signals so that SD, MRC and OC weights can be generated to maximize the SINR of that signal.

MRC weights the signals on each antenna by the reciprocal of the noise power on the corresponding antennas. It then co-phases the component of the desired signal on each antenna and adds them together. Since the pilot-weighted path gains at various PN offsets are readily available, the desired signal was chosen as a pilot signal having a particular PN offset. The desired pilot signal is thus the one whose sum total received power on both antennas is the strongest amongst all the other received pilot signal. We define a vector element $d_{i,m}$ of vector $\mathbf{d}_m \epsilon \{0,1\}$ for antenna m such that

$$d_{i,m} = \begin{cases} 1 & \forall_j \sum_{1 \le m \le M} |a_{i,m}|^2 \ge \sum_{1 \le m \le M} |a_{j,m}|^2, \\ 0 & \text{otherwise} \end{cases} \tag{4.11}$$

Another way of selecting the desired signal is to choose the pilot signal with the strongest received power on any single antenna. This second choice would not take advantage of MRC's ability to increase the desired signal power by co-phasing and adding the desired signal components on both antenna. In this case the vector $\mathbf{d_m}$ would have had elements

$$d_{i,m} = \begin{cases} 1 & \forall_j |a_{i,m}|^2 \ge |a_{j,m}|^2, \\ 0 & \text{otherwise} \end{cases} \tag{4.12}$$

The MRC weights can be represented mathematically as

$$\mathbf{w}_{MRC} = \mathbf{R}_{MRC}^{-1}\mathbf{c} \tag{4.13}$$

where $\mathbf{R}_{MRC} = \begin{bmatrix} \sigma_{n,1}^2 & 0 \\ 0 & \sigma_{n,2} \end{bmatrix}$ is the matrix containing the assumed white noise plus interference powers at each antenna on the leading diagonal and zeros elsewhere, $\mathbf{c}$ is the vector containing the complex fading coefficient of the desired signal due to multi-path fading, time delay, and channel distortions. This is proportional to the pilot-weighted path gain, $\mathbf{a}$. Given a particular pilot signal with a given PN offset, the total interference plus noise power includes detected pilot power, non-detected sync, paging, and traffic power from other interfering sectors and time delayed versions of the pilot signal showing up at different PN offsets. The desired sector's sync, paging, and traffic channels do not contribute to interference power because the sync, paging, and traffic channels are orthogonal to the pilot signal by virtue of the orthogonal Walsh codes used to cover the forward link channels.

Although the total received (signal plus noise plus interference) power at a particular antenna is readily available, the method used to obtain the complex path gains does not yield the total noise and interference powers To obtain the interference power requires knowledge of the power radiated in the sync, paging, and traffic channels of each interfering sector's pilot signal. In fact, to obtain the sync, paging, and traffic power radiated by any given sector is computationally expensive. The sync, paging, and traffic channel powers would have to be calculated in the following manner: for each of the 62 LongCodeMasked Walsh Channels (this excluded the sync and pilot channels) , first de-cover the channel using the Walsh Function, then cycle though the 2^{41} possible delays of the Long PN sequence the particular sector might be using as the LongCodeMask. Clearly this is computationally arduous. The interference power was approximated by the total pilot power received from interfering sectors ($\sum_{\forall_{n,n\neq n_d}} |a_{n,m}|^2$). Since only the relative magnitude of the interference plus noise power at either antenna is important. The noise power was also approximated. An

additive white noise power of 10^{-10} was used to account for internal and external additive white noise. A multiplicative noise power of -20 dB was added to account for digitizing errors when the received RF signal is sampled. The estimate used for the MRC weight vector was thus

$$\mathbf{w}_{MRC} = \frac{\mathbf{R}_{MRC}^{-1}\left(\mathbf{a}\mathbf{d}^{T}\right)}{\left|\mathbf{R}_{MRC}^{-1}\left(\mathbf{a}\mathbf{d}^{\mathbf{T}}\right)\right|} \tag{4.14}$$

where

$$\mathbf{R}_{MRC1} = \begin{bmatrix} 1.05\mathbf{a}_{:,\mathbf{1}}\mathbf{a}_{:,\mathbf{1}}^{\mathbf{H}} - a_{n_d,1}a_{n_d,1}^{*} + 10^{-11} & 0 \\ 0 & 1.05\mathbf{a}_{:,\mathbf{2}}\mathbf{a}_{:,\mathbf{2}}^{\mathbf{H}} - a_{n_d,2}a_{n_d,2}^{*} + 10^{-11} \end{bmatrix},$$

and $\mathbf{a}_{:,\mathbf{m}}$ represents the column vector containing pilot-weighted complex path gains of all detected pilots in a particular fixed order; n_d corresponds to the PN offset of the desired detected pilot signal whose SNR is to be maximized.

Another approximation for noise plus interference power involves using the total received power minus the received desired pilot power. This approximation over estimates the interference and noise power because the desired pilot's corresponding sync, paging, and traffic channel (which are code-orthogonal to the desired pilot signal and thus provide no interference) are included in the interference term. If this approximation hsa been used, then the approximate noise plus interference power at each antenna would have been $\mathbf{R}_{MRC2} = \begin{bmatrix} |v_{1,k}|^2 & 0 \\ 0 & |v_{2,k}|^2 \end{bmatrix}$.

4.2.4 Estimation of OC weight vector

The weight vector generated by the Weiner-Hopf solution is

$$\mathbf{w}_{OC} = \mathbf{R}_{nn}^{-1}\mathbf{c} \tag{4.15}$$

The noise plus interference cross correlation matrix could not be estimated directly. This restriction arose because the data logged contained mostly the in-phase component of the received signal. In fact, if there was no frequency fluctuation in the sampling clock and no phase offset due to the propagation environment, mixing the received signal down to 70MHz and sampling at 5MHz would have left only the in-phase component of the receive signal; the complex path gain would not have been be extract-able from the data.

Although the complex path gains were extracted from the logged data, there was something lost in the way the voltage waveforms are logged. The total received signal cross correlation matrix $\mathbf{R}_{xx}$, required to generate the weight vector using $\mathbf{w}_{OC} = \mathbf{R}_{xx}^{-1}\mathbf{c}$ at the OC combiner, could not be obtained. However, the important metric in OC weight generation is the relative magnitude and phase of each term in the matrix, $\mathbf{R}_{nn}^{-1}$ and $\mathbf{R}_{xx}^{-1}$. An estimate of $\mathbf{R}_{nn}^{-1}$ was employed using the pilot-weighted complex path gains. The noise power was also approximated. An additive white noise power of 10^{-11} was used to account for internal and external additive noise. A multiplicative noise power of -20 dB was added to account for digitizing errors when the received signal was sampled. The noise terms were chosen from knowledge of the noise floor of the measuring device used. Therefore an approximation to the OC weight vector used is

$$\mathbf{w}_{OC} = \frac{\mathbf{R}_{nn}\left(\mathbf{a}\mathbf{d}^{T}\right)}{\left|\mathbf{R}_{nn}\left(\mathbf{a}\mathbf{d}^{T}\right)\right|^{2}} \tag{4.16}$$

where $\mathbf{R}_{MRC} = \begin{bmatrix} 1.05\mathbf{a}_{:,\mathbf{1}}\mathbf{a}_{:,\mathbf{1}}^{\mathbf{H}} - a_{n_d,1}a_{n_d,1}^{*} + 10^{-10} & \mathbf{a}_{:,\mathbf{1}}\mathbf{a}_{:,\mathbf{2}}^{\mathbf{H}} - a_{n_d,1}a_{n_d,2}^{*} \\ \mathbf{a}_{:,\mathbf{2}}\mathbf{a}_{:,\mathbf{1}}^{\mathbf{H}} - a_{n_d,2}a_{n_d,1}^{*} & 1.05\mathbf{a}_{:,\mathbf{2}}\mathbf{a}_{:,\mathbf{2}}^{\mathbf{H}} - a_{n_d,2}a_{n_d,2}^{*} + 10^{-10} \end{bmatrix}$ is the estimate of the noise plus interference cross correlation matrix.

4.2.5 SINR Estimation at Combiner Output

After the MRC and OC weight vectors were estimated, the weights were applied to the logged data and combined. The combined digitized samples were downsampled

to Chipx1, and correlated with the standard PN sequence to obtain the desired and interference pilot powers as illustrated in figure 4-4. The SINR of the strongest pilot was estimated. Let Ps be the desired pilot signal power with a particular $PNoffset_d$; Por is the sync, paging, and traffic channel power which is code-orthogonal to Ps; P_is is the detected pilot power with $PNoffset \neq PNoffset_d$; P_ior is the detected sync, paging, and traffic channel power of detected interference having $PNoffset \neq PNoffset_d$. The total signals available at the output of the combiner filter output is $Ps + Por + \sum_i P_is + \sum_i P_ior + N$ where N is the total received noise power.

The accurate SINR (desired signal power to co-channel interference and noise power) may be defined as

$$SINR_{actual} = \frac{Ps + Por}{\sum_i P_is + \sum_i P_ior + Ps/20 + N} \tag{4.17}$$

where the $Ps/20$ term is added to limit the SINR to a maximum of 13 dB.

P_ior and Por are computationally difficult to estimate. Thus the SINR used in the result is an approximation of equation 4.17 and is defined as

$$SINR_{estimate} = \frac{Ps}{\sum_i P_is + Ps/20 + N_{estimate}} \tag{4.18}$$

The effect of using $SINR_{estimate}$ instead of $SINR_{actual}$ to report the SINR gains is analysed.

Accuracy of SINR Approximation

The accuracy of $SINR_{estimate}$ in estimating $SINR_{actual}$ can be written as

$$\frac{SINR_{estimate}}{SINR_{actual}} = \frac{Ps}{Ps + Por} \frac{\sum_i P_is + \sum_i P_ior + Ps/20 + N}{\sum_i P_is + Ps/20 + N_{estimate}} \tag{4.19}$$

$$= \frac{1}{1 + Por/Ps} \frac{1 + \frac{Ps/20+N}{\sum_i P_is} + \frac{\sum_i P_ior}{\sum_i P_is}}{1 + \frac{Ps/20+N_{estimate}}{\sum_i P_is}} \tag{4.20}$$

which if $N_{estimate} = N$ simplifies to

$$\frac{SINR_{estimate}}{SINR_{actual}} = \frac{1}{1+a_0}\left(1+\frac{1+\sum_i fp_i a_i}{1+\frac{Ps/20+N_{estimate}}{\sum_i P_i s}}\right) \tag{4.21}$$

where $a_i = \frac{P_i or}{P_i s}$ is the ratio of power transmitted on the sync, paging, and traffic channel relative to power transmitted on the pilot channel and is related to how many traffic channels are in use on a particular sector $fp_i = \frac{P_i s}{\sum P_i s}$ is the fraction of total interference pilot power that originates from a particular sector with $PNoffset = PNoffset_i$

The numerator term is just the weighted mean of the ratio of paging, sync, and traffic channel power to pilot channel power from all detected interfering sectors. The numerator is a function of the load on the detected sectors and should be independent of the combining scheme used.

In a noise limited environment, $N_{estimate} >> P_s$, the above equation simplifies to

$$\frac{SINR_{estimate}}{SINR_{actual}} \approx \frac{1}{1+a_0}\left(1+\frac{1+\sum_i P_i s \sum_i fp_i a_i}{N_{estimate}}\right) \tag{4.22}$$

Since interference power is reduced in OC and is increased in MRC, the use of $SINR_{estimate}$ in a noise limited environment, leads to an overestimation of the MRC SINR gains but an underestimation of the OC SINR gains.

In an interference limited environment, $\sum_i P_i s >> N_{estimate} + P_s/20$, the above equation simpilies to

$$\frac{SINR_{estimate}}{SINR_{actual}} \approx \frac{1}{1+a_0}\left(1+\sum_i fp_i a_i\right) \tag{4.23}$$

In interference limited region, as none of the terms in this equation are affected by the combining scheme, the reported SINR gains are not affected by approximation of $SINR_{actual}$ using $SINR_{estimate}$.

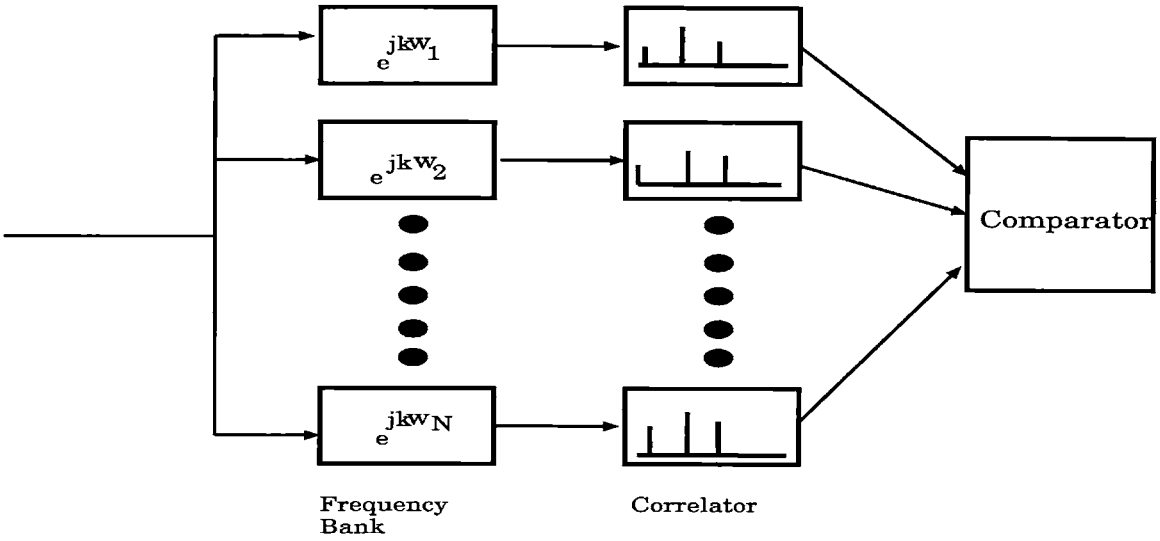

Figure 4-6: Frequency searcher

In an environment where $Ps >> N$

$$\frac{SINR_{estimate}}{SINR_{actual}} \approx \frac{1}{1+a_0}\left(1+\frac{1+\sum_i P_i s \sum_i fp_i a_i}{Ps}\right) \tag{4.24}$$

Both desired signal and interference power are reduced in OC and interference power is increased using MRC, therefore in an environment where $Ps >> N$, the use of $SINR_{estimate}$ in this report leads to an overestimation of the MRC SINR gains but an underestimation of the OC SINR gains.

4.3 Data Processing Limitations

4.3.1 Frequency Error

The first step in processing the logged data was to run it through a frequency searcher. (See figure 4-4). The frequency searcher does a search in frequency space to find the residual rolling rate of the pseudo-random noise signal (PN code) through the baseband samples. This residual roll has its origins in the inexact downconversion to baseband. The residual frequency ω_e is the output of the frequency searcher.

Figure 4-6 illustrates the steps used to find the residual frequency ω_e. The process is simple. The digitized samples are multiplied by a bank of frequencies ω_r; the output of each frequency bank component is passed through a correlator that generates the pilot weighted complex path gains and equivalently the pilot powers for each of the 2^{15} PN offsets. Given the pilot powers at each PN offset the comparator collects the maximum pilot power from applying each frequency offset. The comparator then performs parabolic estimation to determine the particular frequency $\omega_r = \omega_e$ that maximizes the detected pilot power.

In the methods used to generate the MRC and OC weights, it is assumed that the sampling clock's frequency error from 5MSps is fixed. However, during data processing, the sampling clock's frequency error δf was found to fluctuate slowly from sample to sample. This resulted in loss of detected pilot power accuracy. A way to more accurately measure pilot powers is to perform the frequency search for each digitized sample on every logged antenna since it was discovered that the standard deviation of sampling clock's frequency error between samples in time was the sameas the standard deviation between samples on different atennas. This corrective measure, however, would increase processing time by many orders of magnitude. The frequency error was therefore averaged using the first 100 samples; the average frequency error was used to approximate the time dependent frequency error for subsequent samples. This method resulted in a 0 to 1.6 dB loss in detected pilot power.

The estimation error in ω_e affects MRC and OC weight generation and is expected to reduce the reported MRC and OC SINR gains so that what can be expected using more accurate means, would exceed what is reported here.

4.3.2 Detected Pilot Power Smearing Across PN offsets

Figure 4-7 shows the method used to despread the pilot signals from the digitized samples. After the frequency error was found using the frequency searcher the samples were downsampled to the Chipx1 rate (1228800 Samples per second) using linear

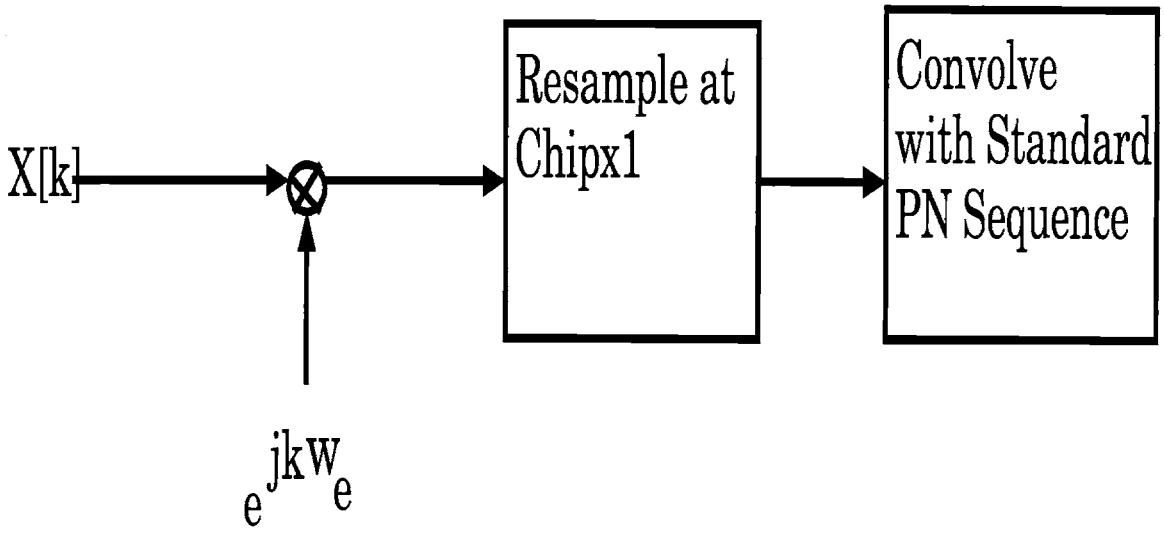

Figure 4-7: Pilot signal detector

interpolation before it is convolved with the standard PN sequence. The effect of performing convolutions was to perform multiple correlations with the standard PN sequence having varing delays. This captured the energy of pilot signals at all 2^{15} possible PN sequence offsets with Chipx1 accuracy.

Because of the non zero path lengths from the transmitting base station sector to the handset receiver, the PN offset of the received pilot is shifted sometimes by fractions and at other time by whole chip durations from the sector's PN offset at transmission. To detect the complex path gain of a particular sector's pilot signal the standard sequence correlated with the base station's pilot signal, should be such that it's delay is precisely aligned with that of the received pilot signal (ie. $t_{probe} = \tau_n - t_{i,n,m}$). Any misalignment means that the pilot power detected at a particular PN offset will smear into adjacent PN offsets.

IS-95 standard suggests using an early-late gate mechanism to ensure that most of the pilot's energy is localized in it's detected PN offset and as little as possible smears across adjacent PN offsets. Applying this mechanism to all detected pilot signals using all concieved approaches that do not require decoding the Sync Channel is computationally expensive - the suggestion is abandoned.

Therefore parameter estimation inaccuracies occur if the misalignment of a particular

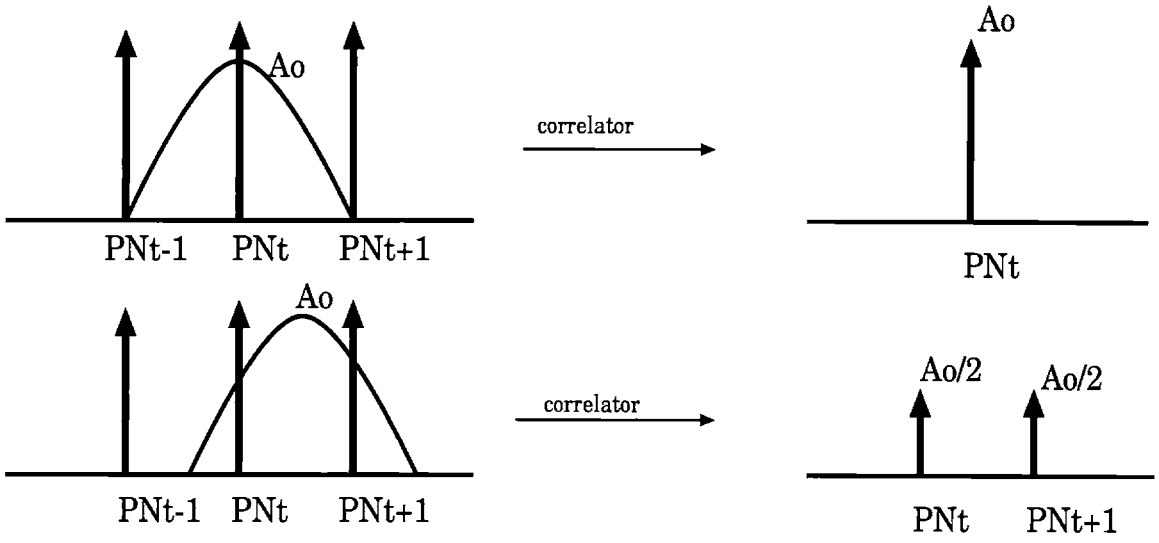

Figure 4-8: Detected pilot power smearing across PN offsets

sector's transmitted pilot signal with the standard PN sequence is not precisely a constant multiple of the chip duration. The magnitude of the error increases from 0 to half the detected pilot's power as the misalignment increases from zero to half a chip duraction. (See Figure 4-8). Therefore an inaccuracy is that the pilot powers detected in a particular PN offset (PNt) may either be (1) the total pilot power from a pilot signal or (2) a fraction of the total power from a pilot whose energy is smeared across multiple PN offsets. (PN_t and PN_{t-1} in figure 4-8).

As a result of pilot power smearing, the desired pilot's complex path gain at a particular antenna might be underestimated and the noise power might be overestimated. For, the desired pilot power leaks into another PN Offset and tends to be detected as an interferer. Clearly this adversly effects the precision of the SD, MRC and OC weights in that order of severity. This estimation error is expected to further reduce the reported SINR gains so that what can be expected from antenna diversity combining using more accurate means should exceed what is reported here.

The smearing of the pilot powers is not accounted for in the weight generation for SD,MRC, and OC weights, but it is accounted for in the SINR and output power results presented. The way the pilot power smearing is accounted for is by assuming that all pilot signals detected at adjacent PN offsets are a result of pilot power smear-

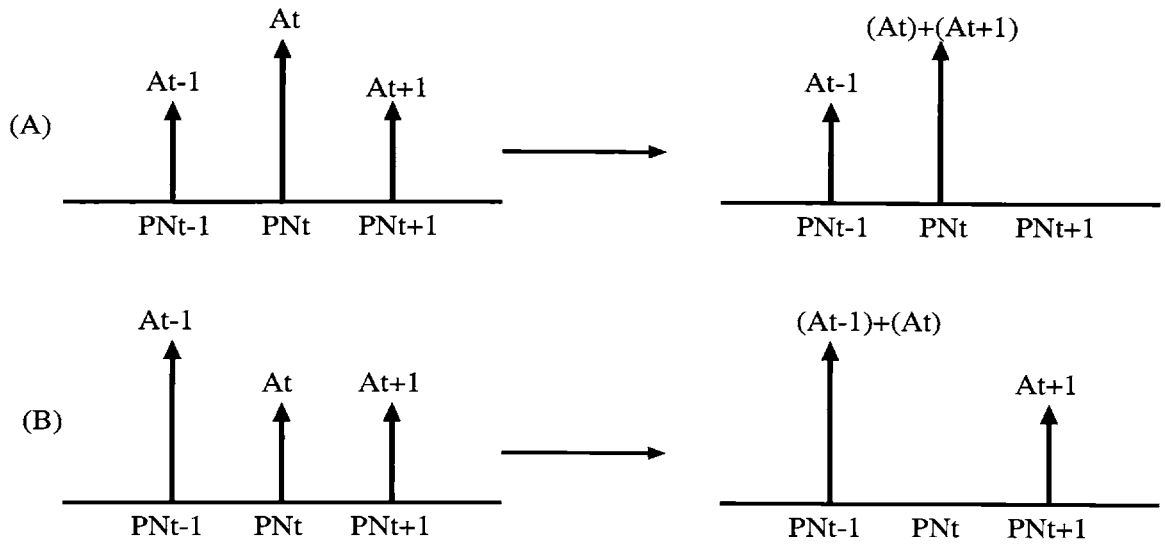

Figure 4-9: Corrective measure for Pilot Power Smearing

ing. (See figure 4-9). A problem resulting from this corrective measure is that in some cases actual interference signal powers might be wrongly reported as desired signal power. For example, from figure 4-9, an error occurs if A_0 and A_2 are not a result of pilot power smearing. The assumption used to account for pilot power smearing affects the SINR and power reported for the two receive antennas, SD, MRC, and OC to the same extent. Thus, the SINR gains are not affected.

4.3.3 Summary

In conclusion, the above limitations in the accuracy of the frequency error (ω_e) and the pilot power estimations means that the results presented here are not an upper-bound on the SINR gains obtainable. Errors in w_e and pilot power estimation affect OC in two ways. First the noise and interference cancellation capabilities of OC are reduced because of errors in the parameter estimation of the pre-whitening filter (R_{nn}^{-1}). Correlted intererence plus noise is not properly co-phased when their cancellation is attempted. Second, the desired signal's components at the two antennas cannot be accurately co-phased when they are added together. The desired signal's power cannot be amplified in an optimal way. Thus, SINR gains expected from antenna diversity combining using more accurate should exceed what is reported here.

Chapter 5

Antenna Diversity Measurement Results and Analysis

5.1 In-Laboratory Trials

Experiments were conducted in lab to test the accuracy of the methods used to estimate channel parameters. This was done by verifying that the estimates used to generate MRC and OC weights produced SINR gains that were consistent with theoretical predictions.

5.1.1 Experimental setup

A standard pseudo-random noise CDMA base station signal generator (Techtronix CMD80) was connected to a TAS 4500 channel simulator. The channel simulator superposed Rayleigh fading characteristics onto the CDMA base station signals and provided maximum Doppler shifts of 20Hz, 30Hz, and 50Hz to the CDMA signals on two and three multi-path channels. The output of the channel simulator was connected to the measurement device and the RF signals logged.

Experiments were performed using two and three multi-paths at each antenna chan-

nel. Where appropriate these paths are referred to as path1, path2, path3 respectively. Doppler shifts along the paths were set to 20Hz, 30Hz, 50Hz respectively; and path loss was set to 0dB, 3dB and 6dB respectively. Figures 5-1, 5-4, 5-7, and 5-10 are cumulative distribution functions (CDF) of the SINR estimates of the maximum power pilot signal on the two receive antennas, a combined signal using Selection Diversity (SD), a combined signal using Maximum Ratio Combining (MRC), and a combined signal using Optimum Combining (OC) on logged data.

In literature on CDMA signals it is desirable that the antenna system guarantee a certain minimum SINR 90%, , 95%, and 99% of the time. This minimum SINR corresponds to the 10^{-1}, $5 * 10^{-2}$, and 10^{-2} mark on the CDF plots presented. The SINR gain 90%, 95%, and 99% of the time, in decibels, is the difference between the SD and the right most antenna curve at the 10^{-1}, $5*10^{-2}$, and 10^{-2} marks respectively, the SINR gains in decibels of MRC 90%'tile, 95%'tile, and 99%'tile is the difference between the MRC curve and right most SINR curve of the dual antennas at the 10^{-1}, $5 * 10^{-2}$, and 10^{-2} marks respectively; the SINR gain using OC is similarly defined.

The settings for Doppler shift, cross correlation, delay, path loss, and envelope correlation coefficient of signals at the two antennas as set in the channel simulator are tabulated in tables 5.1 and 5.2.

	Lab Test1	**Lab Test1**	**Lab Test2**	**Lab Test2**
	Path1	**Path2**	**Path1**	**Path2**
Path Loss	0	3	0	3
Delay μs	0	10	0	10
Doppler Shift (Hz)	20	30	20	30
Env. Cross. Corr.	0	0	1	1

Table 5.1: Channel Settings for Lab Test 1 and Test 2

	Lab Test3	Lab Test3	Lab Test4	Lab Test4	Lab Test4
	Path1	Path2	Path1	Path2	Path3
Path Loss	0	3	0	3	6
Delay μs	0	10	0	10	100
Doppler Shift (Hz)	20	30	20	30	50
Env. Cross. Corr.	.95	.95	.95	.95	0

Table 5.2: Channel Settings for Lab Test 3 and Test 4

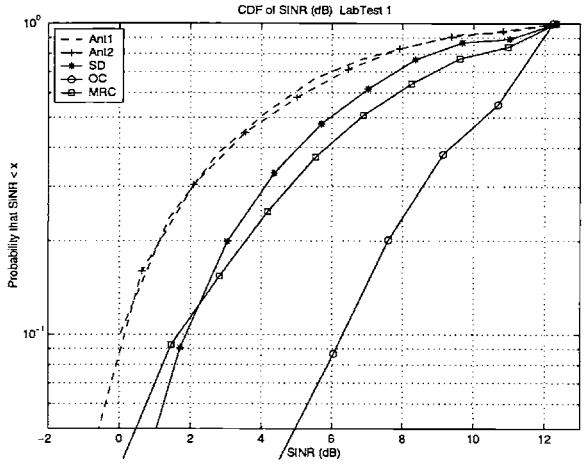

Figure 5-1: CDF of SINR. Lab Test1 using two paths, 0 env. corr. coeff.

5.1.2 MRC and OC SINR characteristics

Experiment 1

Figures 5-1, 5-2, and 5-3 present, respectively, the SINR, desired pilot signal power, interference pilot power plus noise power for the two path channel with zero long term envelope correlation. The diversity gain (SD SINR gain) is approximately 1.8dB at the 95%'tile, and 2dB at the 90%'tile. The MRC SINR gain is 1.3dB at 95%'tile and 1.8dB at 90%'tile. OC SINR gain is 5.8 dB at the 95%'tile and 6.2dB at the 90%'tile . The reason for the large OC SINR gain is evident from figures 5-2 and 5-3 and related to equation 2.39. Clearly, the $\Re\left(\rho_s(n)^*\rho_s(s)\right)$ term must be very low since there is little signal power cancellation. Although the long envelope correlation coefficient is set to zero, the instantaneous cross correlation of signals must not be zero. From figure 5-3, the $|\rho_s(n)|^2$ term in equation 2.39 leads to more than 5 dB interference power reduction for OC.

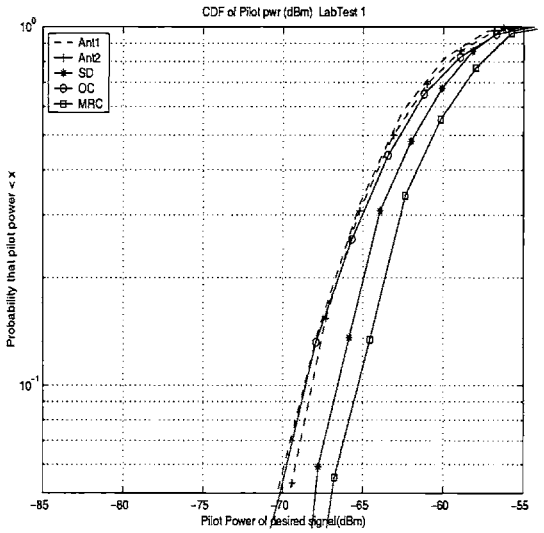

Figure 5-2: CDF of Signal Pwr. Lab Test 1 using two paths, 0 env. corr. coefficient

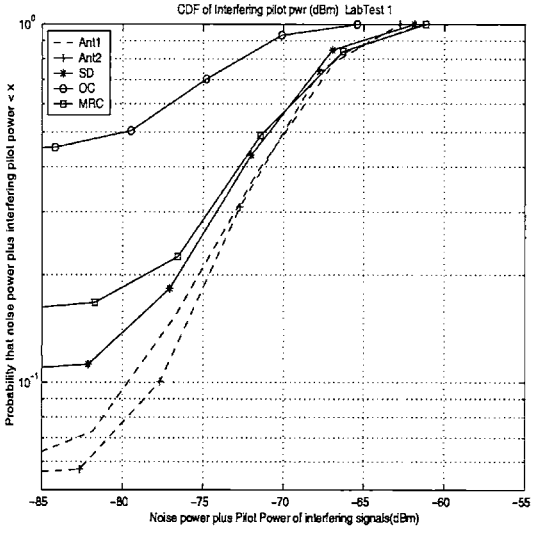

Figure 5-3: CDF of Interference Pwr. Lab Test 1 using two paths, 0 env. corr. coefficient

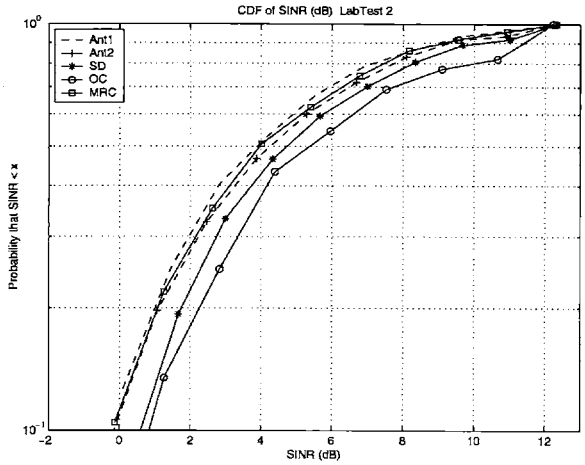

Figure 5-4: CDF of SINR. Lab Test 2 using two paths. 1,1 env. corr. coeff.

Lab Test 2

Figures 5-4, 5-5, and 5-6 present, respectively, the SINR, desired pilot signal power, interference pilot power plus noise power for the two path channel with 100% long term envelope correlation. Data is only available at the 90%'tile. The SINR gains are very low as expected. The diversity gain is approximately 0.6dB dB. The MRC SINR gain is 0dB; the OC SINR gain is 0.8dB. The reason for 0dB MRC SINR gain, and the correspondingly low OC SINR gain is deducible from figures 5-5 and 5-6 and using equation 2.39. Clearly the $\Re\left(\rho_s(n)^*\rho_s(s)\right)$ must be very high since MRC has a large interference power and noise amplification. This is not overcome by the gain in signal power from using MRC combining, resulting in the 0dB SINR gain. The 0.8dB OC SINR gain is a result of large signal cancellation from the high $\Re\left(\rho_s(n)^*\rho_s(s)\right)$ term; and a large compensating interference cancellation, from correlated interference terms at the antenna ports (high $|\rho_s(n)|^2$ term).

Lab Test 3

Figures 5-7, 5-8, and 5-9 present, respectively, the SINR, desired pilot signal power, interference pilot power plus noise power for the two path channel with 95% long term envelope correlation. Data is only available at the 90%'tile. The diversity gain

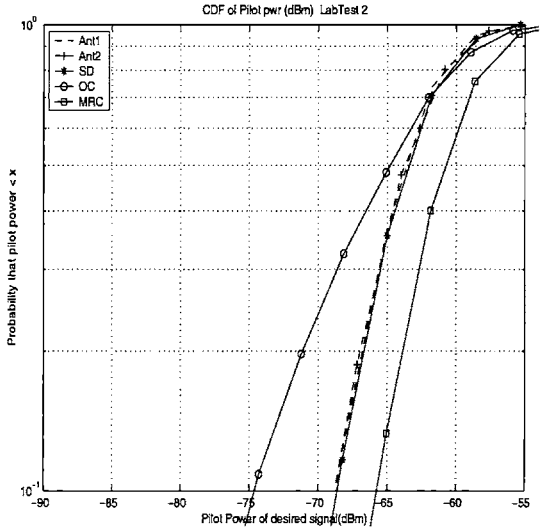

Figure 5-5: CDF of Signal Pwr. Lab Test 2 using two paths. 1,1 env. corr. coeff.

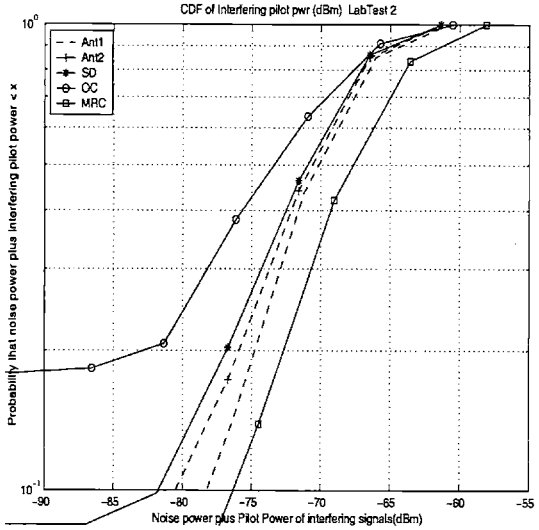

Figure 5-6: CDF of Interference Pwr. Lab Test 2 using two paths. 1,1 env. corr. coefficient

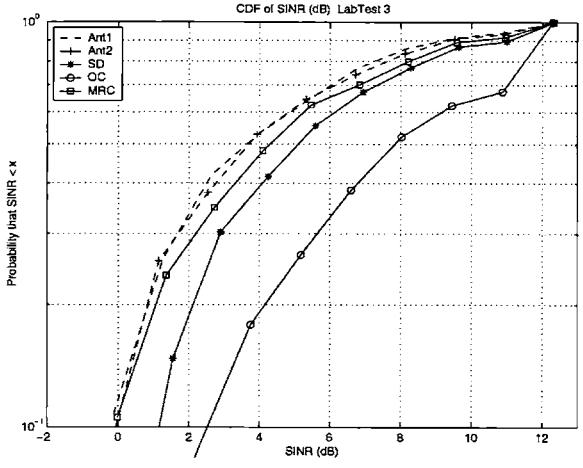

Figure 5-7: CDF of SINR. LabTest 3 using two paths. 0.95, 0.95 env. corr. coeff.

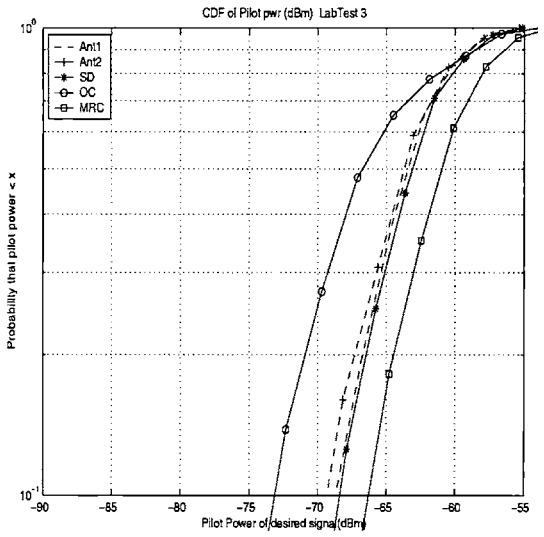

Figure 5-8: CDF of Signal Pwr. Lab Test 3 using two paths. 0.95, 0.95 env. corr. coeff.

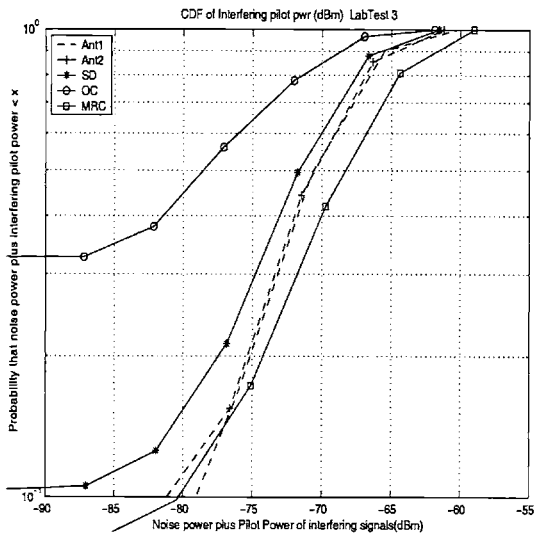

Figure 5-9: CDF of Interference Pwr. Lab Test 3 using two paths, 0.95,0.95 env. corr. coefficient

is approximately 1.2dB. The MRC SINR gain is 0dB; the OC SINR gain is 2.6dB. The reason for 0 dB MRC SINR gain is because although it has a 3dB pilot power gain over SD, it has about a 3dB interference power and noise power amplification above that of SD. Clearly the $\Re\left(\rho_s(n)^*\rho_s(s)\right)$ must be relatively high since high MRC noise plus interference power amplification is accompanied by a 5dB signal power cancellation by OC. Interference cancellation by OC (related to the $|\rho_s(n)|^2$ term from correlated interference and noise at the antennas) more than compensates for the reduced signal power.

Lab Test 4

Figures 5-10, 5-11, and 5-12 differ from Figures 5-7, 5-8, and 5-9 because Lab Test 4 includes one more multi-path component than Lab Test 3 whose cross correlation coefficient at the two antennas is zero. The diversity gain in this case is 1.2dB. The MRC SINR gain is 0.6dB; the OC SINR gain is 1.8dB. The reason for the higher MRC SINR gain is because of the lower noise plus interference amplification derived from the additional path with zero correlation coefficient. The OC SINR gain is reduced because of the additional multi-path interference.

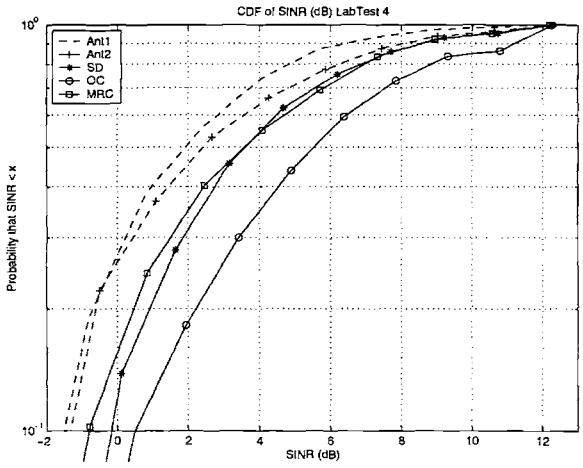

Figure 5-10: CDF of SINR. Lab Test 4 using two paths. 0.95, 0.95 env. corr. coeff.

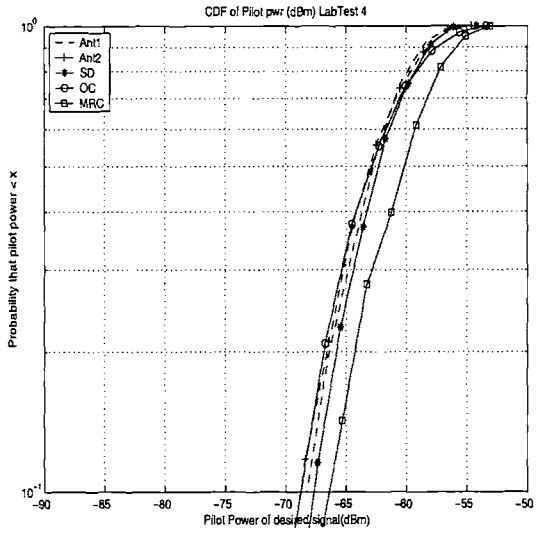

Figure 5-11: CDF of Signal Pwr. Lab Test 4 using two paths. 0.95, 0.95 env. corr. coeff.

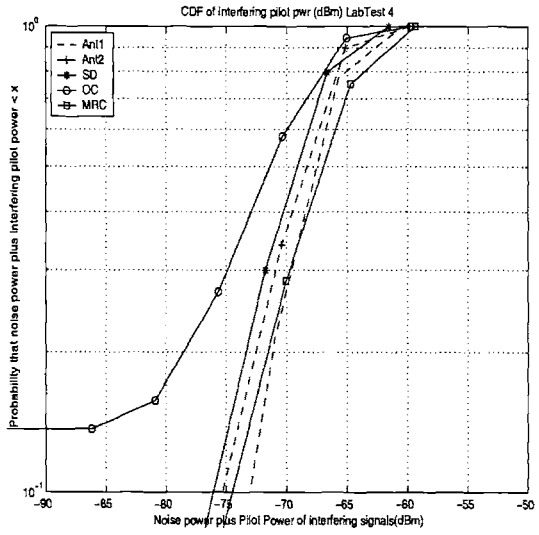

Figure 5-12: CDF of Interference Pwr. Lab Test 4 using two paths, 0.95,0.95 env. corr. coefficient

Name	Description
Area Trial 1	Handset on phantom head dummy facing inside
Area Trial 2	Handset on phantom head dummy facing window
Area Trial 3	Handset held against human operator's head facing inside
Area Trial 4	Handset held against human operator's head facing window

Table 5.3: Downtown trials

8

5.2 Outdoor Measurements

Experiments were conducted with the mobile handset alternatively against the phantom head dummy in the test van and held by a human operator against his head. Table 5.3 describes the different configurations tested. Downtown Trail 1 corresponds to Area Trial 1 conducted in the Downtown Area: The mobile handset was placed on the side of phantom head dummy facing the window. Tests were conducted with the phone on either side of the phantom head dummy to investigate whether the position of the phone in the test van has any effect on the SINR gains. In each case the angle subtended by the handset relative to the vertical axis is maintained.

Since the position of the internal monopole is such that the hand of the human operator partially blocks the internal monopole antenna, human operator trials were conducted to investigate the effects of hand blockage on the performance of the diversity antenna system.

For each Area Trial the output of each of the two antennas was connected to the measurement device and the impinging RF signals simultaneously logged. The SINR of each receive antenna and the output SINR of the SD, MRC and OC combined signals were computed from the logged data during post processing in the Matlab environment.

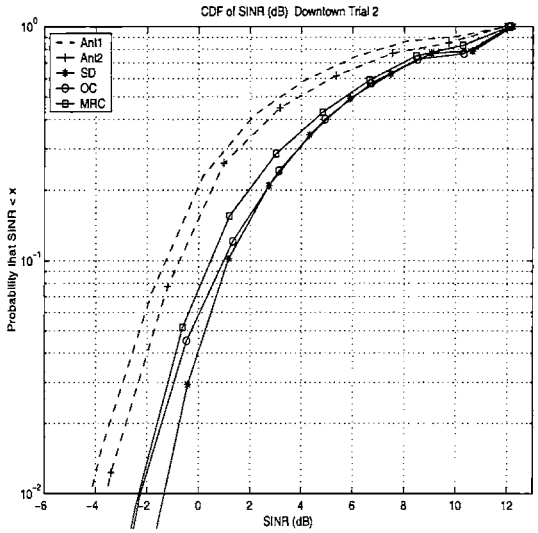

Figure 5-13: CDF of SINR. Downtown: handset on phantom head facing window

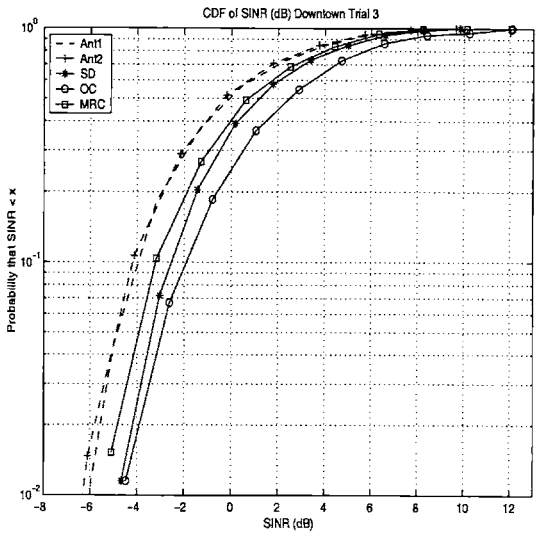

Figure 5-14: CDF of SINR. Downtown: handset held by human operator facing window

5.2.1 Downtown Area

The downtown area trails were conducted along a five minute drive route around the Horton plaza in downtown San Diego. The route starts and terminates at the corner of C Street and 4th Street. The location was chosen with an expectation that the high rise buildings, moving vehicles, and general close-spaced buildings provide a multi-path rich environment.

Figures 5-13, 5-15, and 5-17 corresponds respectively to the SINR, the pilot power (in dBm) of the strongest detected multi-path component, and the total interference signal's pilot power plus a 10^{-10} term added to account for additive noise power when the phantom head dummy is in use; figures 5-14 , 5-16, and 5-18 correspond to the when a human operator holds the mobile handset against his head. The results with the phantom head dummy and with the human operator are juxtaposed to facilitate comparing their characteristics.

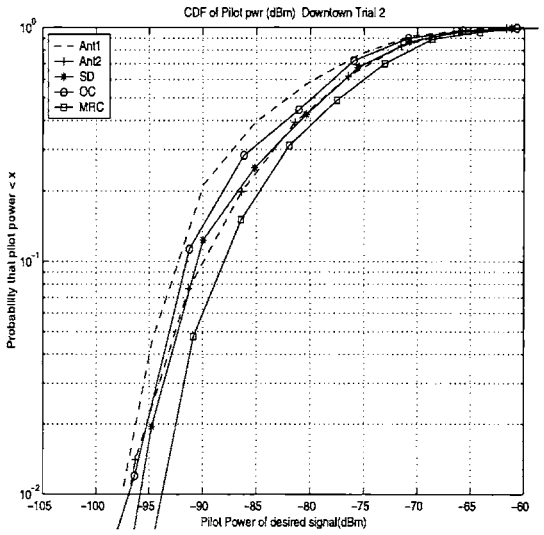

Figure 5-15: CDF of Desired Signal Power. Downtown: handset on phantom head facing window

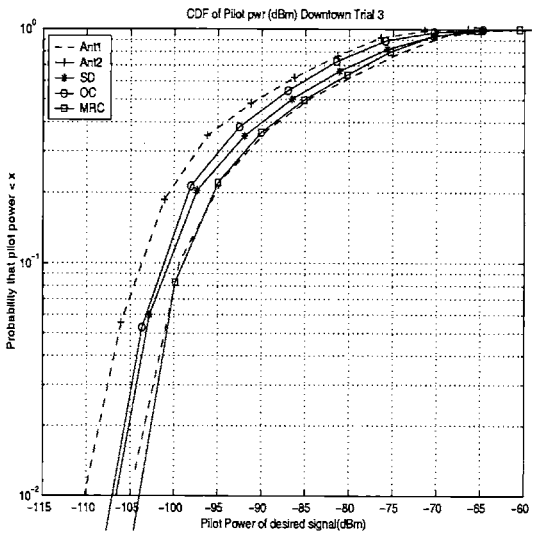

Figure 5-16: CDF of Desired Signal Power. Downtown: handset held by human operator facing window

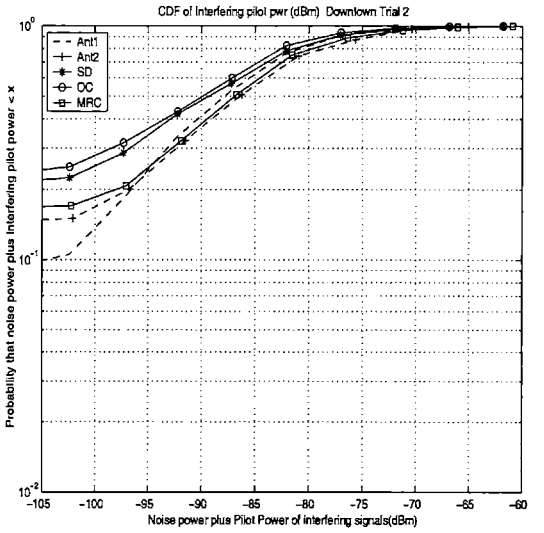

Figure 5-17: CDF of Interference and Noise Power. Downtown: handset on phantom head facing window

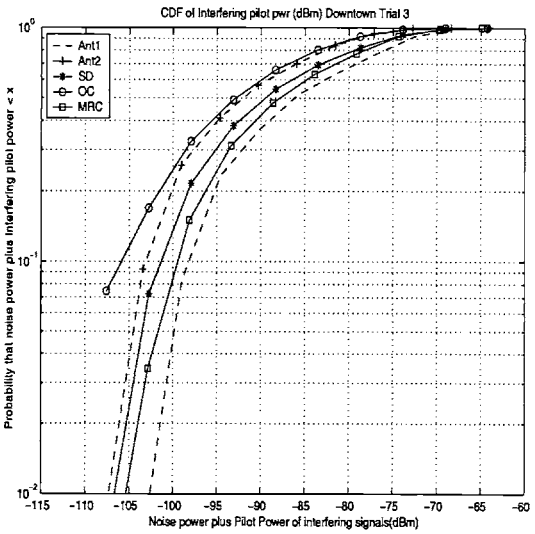

Figure 5-18: CDF of Interference and Noise Power. Downtown: handset held by human operator facing window

Table 5.4: SINR gains of downtown trials with handset facing window; SINR

	Phantom head dummy			*Human operator*		
Percentile	**SD**	**MRC**	**OC**	**SD**	**MRC**	**OC**
90	2.0	1.4	1.8	1.6	0.8	2.0
95	2.0	1.2	1.6	1.6	0.8	2.0
99	1.9	1.4	1.4	1.6	0.8	1.8

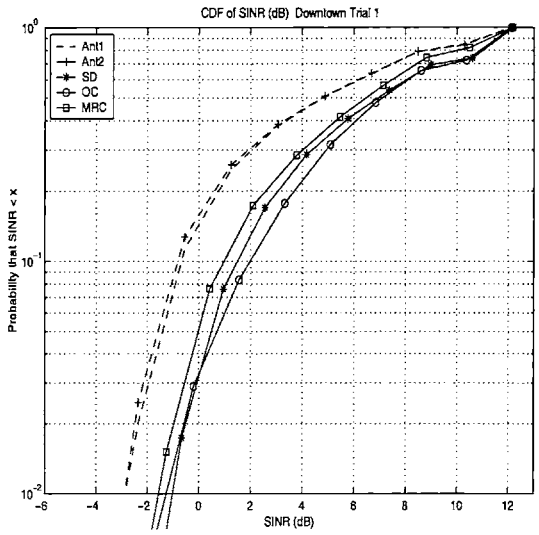

Figure 5-19: CDF of SINR. Downtown: handset on phantom head facing inside

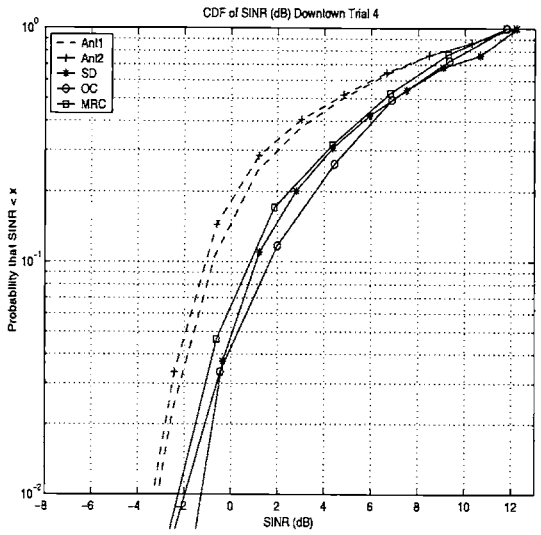

Figure 5-20: CDF of SINR. Downtown: handset by human operator facing inside

Handset next to Window

In cases where the phantom head dummy and the human operator was experimented with, OC guaranteed a SINR gain of above 1.8dB 90% of the time over the best single antenna; SD guaranteed 1.6dB when in use by a human operator and 2.0dB otherwise; MRC, 0.8dB when in use by a human operator and 1.4dB otherwise.

In the downtown area when the handset is facing the window, effect of the human operator's hand blocking the internal monopole antenna is to cause the SD and MRC gains at the 90%tile to fall by 0.4dB but the OC gains to rise by 0.2dB. Figures 5-15 and 5-16, shows that the effect of the human operator's hand is to decrease the received power on the internal monopole 'Ant2' relative to the top mounted monopole antenna 'Ant1'. This increases the mean power difference at the two antennas and degrades the desired signal's power amplificiation that is typical in MRC combining and thus it's gain. SD is also affected in the similar way.

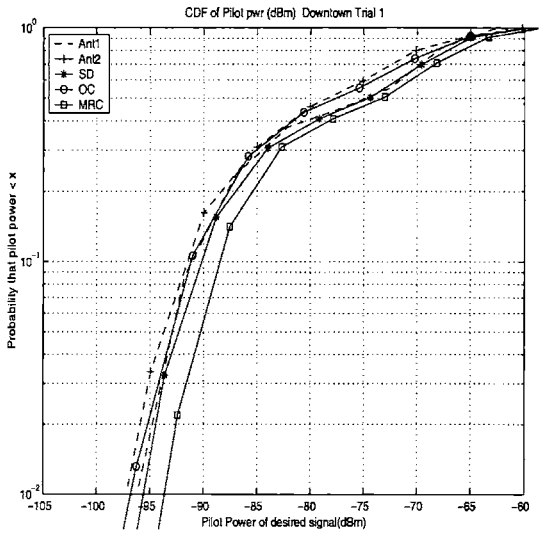

Figure 5-21: CDF of Desired Signal Power. Downtown: handset on phantom head facing inside

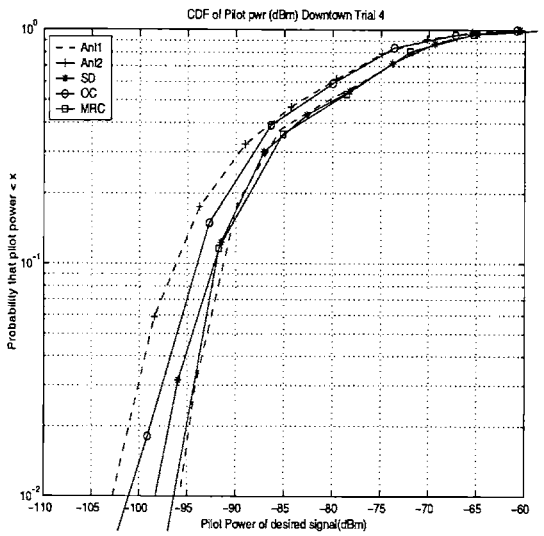

Figure 5-22: CDF of Desired Signal Power. Downtown: handset held by human operator facing inside

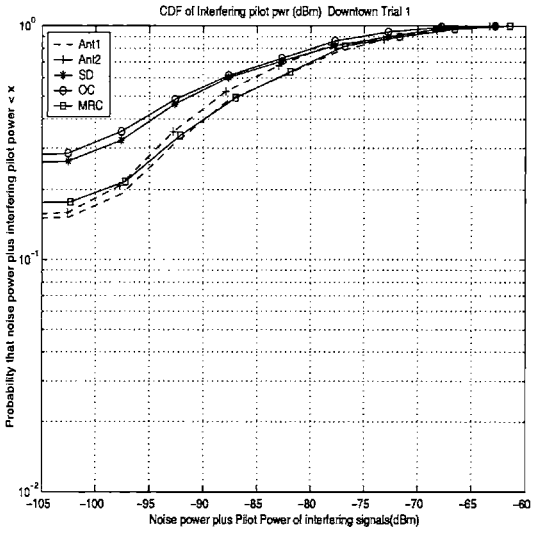

Figure 5-23: CDF of Interference and Noise Power. Downtown: handset on phantom head facing inside

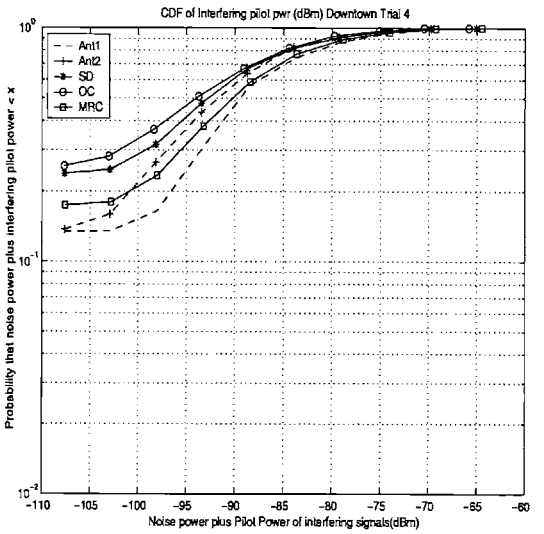

Figure 5-24: CDF of Interference and Noise Power.Downtown: handset held by human operator facing inside

Table 5.5: SINR gains of downtown trials with handset facing inside

	Phantom Head Dummy			*Human Operator*		
Percentile	**SD**	**MRC**	**OC**	**SD**	**MRC**	**OC**
90	2.2	1.6	2.6	1.8	1.0	2.4
95	2.0	1.4	2.2	1.6	1.0	1.8
99	1.8	1.4	2.2	1.2	1.6	2.0

Handset facing inside

In cases where the phantom head dummy and the human operator was experimented with, OC guaranteed respectively a SINR gain of above 2.6dB and 2.4dB, 90% of the time over the best single antenna; SD guaranteed 2.2dB when in use by a human operator and 1.8dB otherwise; MRC, 1.6dB when in use by a human operator and 1.0dB otherwise.

In the downtown area when the handset is facing the inside of the van, effect of the human operator's hand blocking the internal monopole antenna is to cause the SD and MRC gains at the 90%tile to fall by 0.4dB but the OC gains fall by 0.2dB. Figures 5-21 and 5-22, shows that the effect of the human operator's hand is to decrease the received power on the internal monopole 'Ant2' relative to the top mounted monopole antenna 'Ant1'. This increases the mean power difference between the two antennas and degrades the desired signal's power amplificiation that is typical in MRC combining - and thus it's gain. SD is also affected in the similar way.

5.2.2 Open Area

The open area trials were conducted along what is approximately a five minute route that starts at the intersection of miramar street and kearny villa road, goes up kearny villa road, transfers onto kearny mesa road, and ends at the point of departure. The location was chosen with the expectation that the absence (or few) of scatterer in the vicinity of the mobile would result in low levels of multi-path.

Handset facing window

From table 5.6 at the 90%tile SD, MRC, and OC promise 1.4dB, 1.4dB, 1.7dB when used by a human operator and 1.4dB, 1.4dB, and 1.7dB when on the phantom head dummy. The SINR gain of SD and MRC appear not to be affected by the hand blockage of the human operator. Thus, for the open area trials the human operator

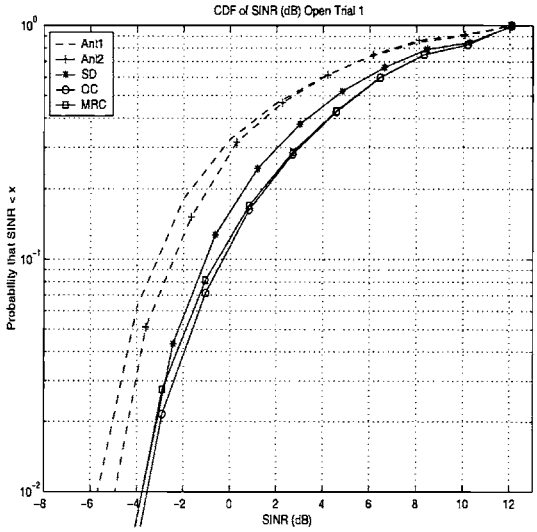

Figure 5-25: CDF of SINR. Open Area: handset on phantom head facing window

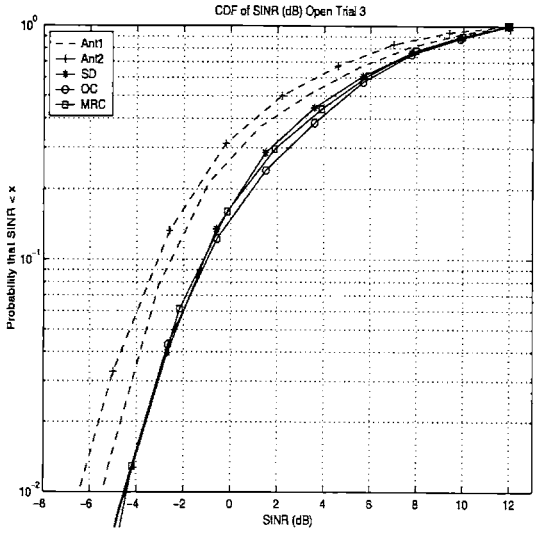

Figure 5-26: CDF of SINR. Open Area: handset held by human operator facing window

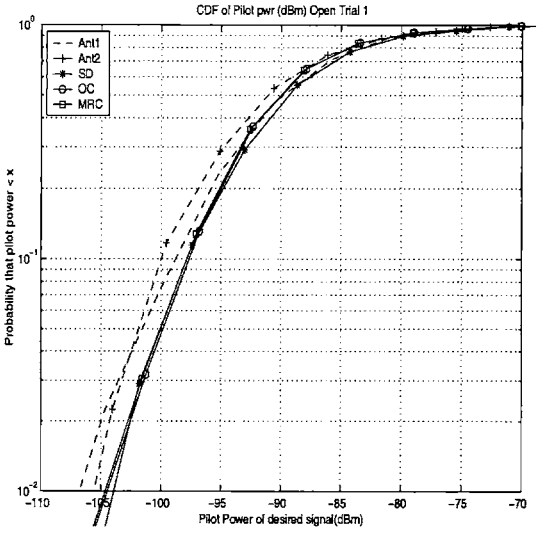

Figure 5-27: CDF of Desired Signal Power. Open Area: handset on phantom head facing window

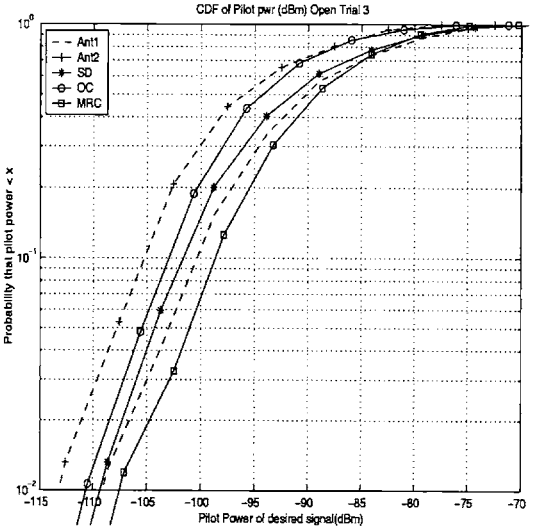

Figure 5-28: CDF of Desired Signal Power. Open Area: handset held by human operator facing window

Table 5.6: SINR gains of Open area trials with handset faincg window

	Phantom Head Dummy			*Human Operator*		
Percentile	**SD**	**MRC**	**OC**	**SD**	**MRC**	**OC**
90	1.4	1.4	1.7	1.4	1.4	1.5
95	1.4	1.2	1.6	1.2	1.2	1.2
99	1.2	1.2	1.4	1.0	1.0	1.0

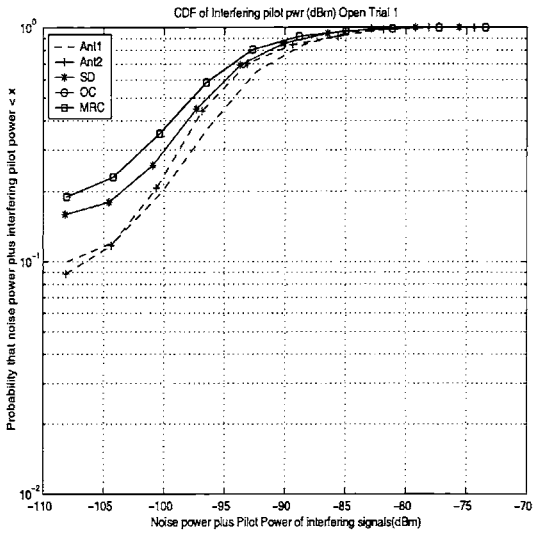

Figure 5-29: CDF of Interference and Noise Power. Open Area: handset on phantom head facing window

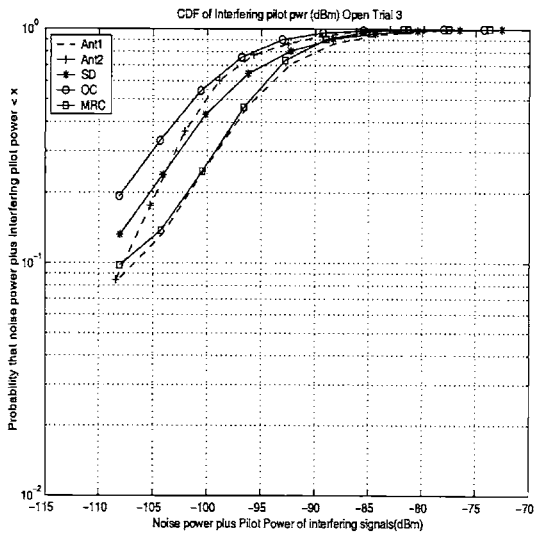

Figure 5-30: CDF of Interference and Noise Power. Open Area: handset held by human operator facing window

Table 5.7: SINR gains of Open area trials with handset facing inside

	Human Operator		
Percentile	**SD**	**MRC**	**OC**
90	1.6	1.6	2.2
95	1.5	1.5	1.7
99	1.5	1.5	2.0

had little if any effects on the SINR gains from SD, OC, and MRC at the 90%'tile.

Handset facing inside

Data is only available for the human operator trials with the handset facing the window. From table 5.7, at the 90%tile, the SINR gain for SD and MRC is 1.6dB but the OC SINR gain is 2.2dB

5.2.3 Residential Area Trials

The residential area trails were conducted along a five minute route in the mira mesa residential area just off mira mesa boulevard. The location was chosen with the

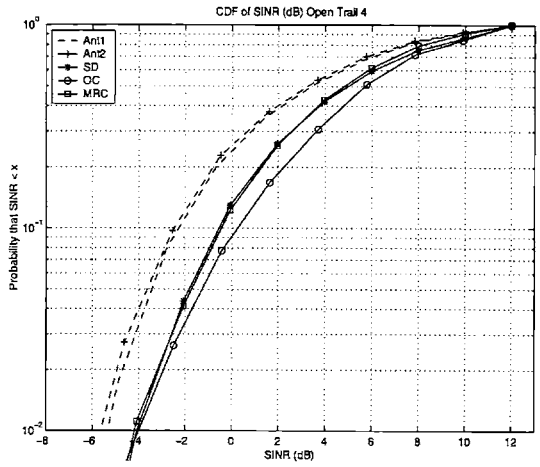

Figure 5-31: CDF of SINR. Open Area: handset on phantom head facing inside

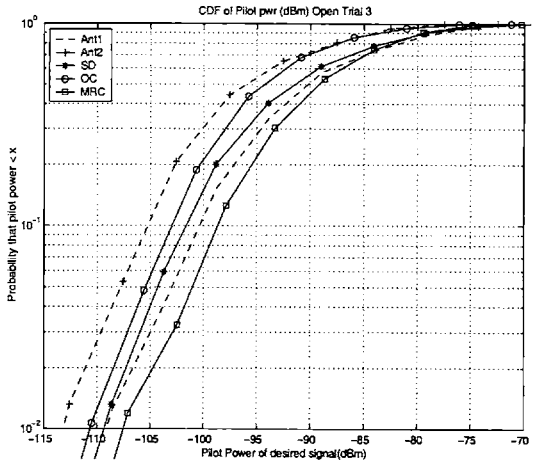

Figure 5-32: CDF of Desired Signal Power. Open Area: handset on human operator facing inside

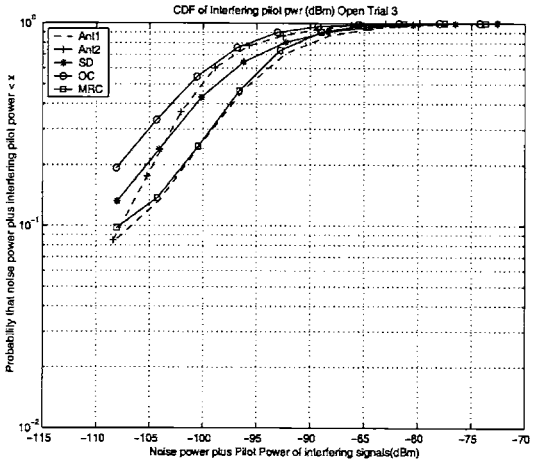

Figure 5-33: CDF of Interference and Noise Power. Open Area: handset on human operator facing inside

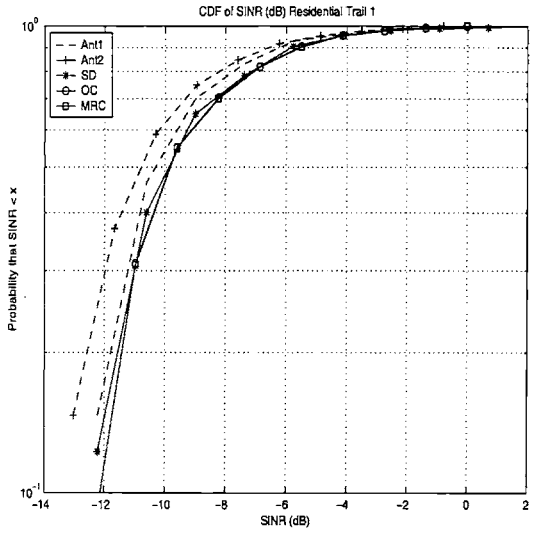

Figure 5-34: CDF of SINR. Residential: handset on phantom head facing window

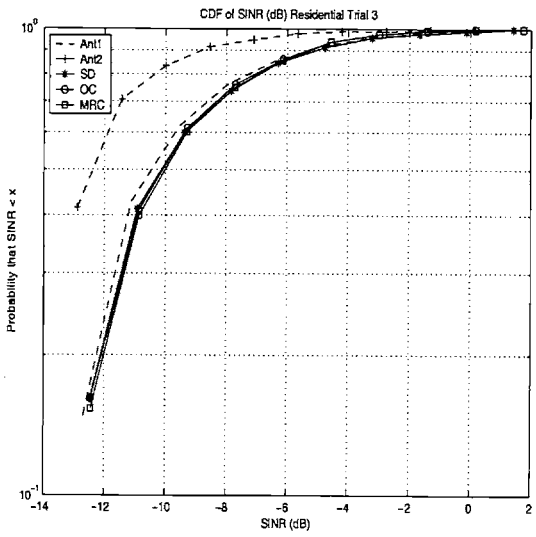

Figure 5-35: CDF of SINR. Residential: handset held by human operator facing window

Table 5.8: SINR gains of residential trials with handset facing window

	Phantom Head Dummy			*Human Operator*		
Percentile	**SD**	**MRC**	**OC**	**SD**	**MRC**	**OC**
90	0.1	0.1	0.1	0.2	0.2	0.2

expectation that the regularly spaced, low height homes would result in result in moderate levels of multi-path.

Handset facing window

Data is only available for the 90%tile. The residential area chosen turned out to be a noise limited regime. The strongest pilot signal was usually of weak strength and there was a large SINR difference existed between signals received on the two antennas. The internal monopole's pilot signal strengths were orders of magnitude weaker than those of the top mounted monopole. This can be attributed to the observation that most of the time the directional internal monopole antenna was pointing in the wrong direction and thus unable to pick up signals from the serving base station. The power difference and large magnitude of noise to interference signal power resulted in significant SINR difference between the two antenna chains. In

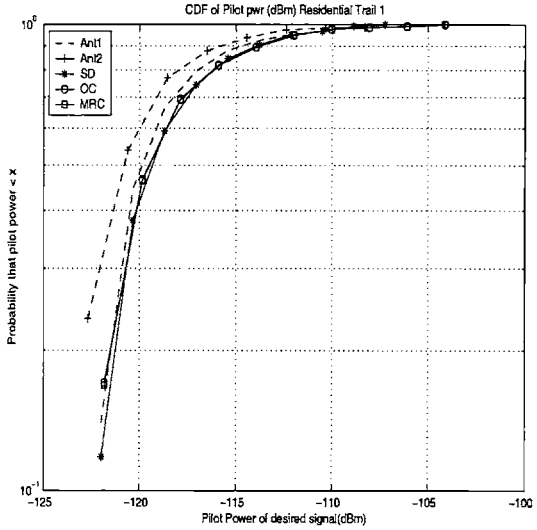

Figure 5-36: CDF of Desired Signal Power. Residential: handset on phantom head facing window

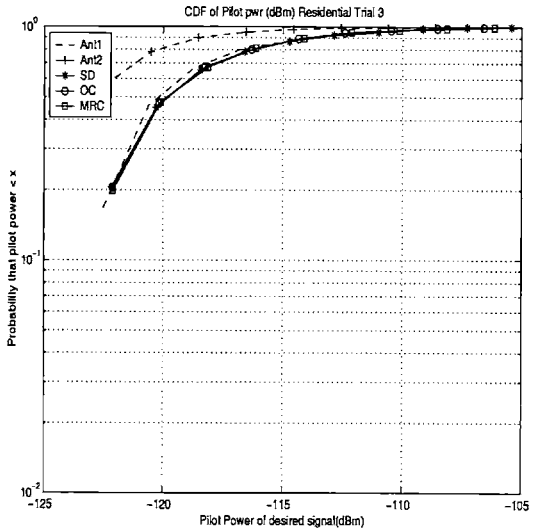

Figure 5-37: CDF of Desired Signal Power. Residential: handset held by human operator facing window

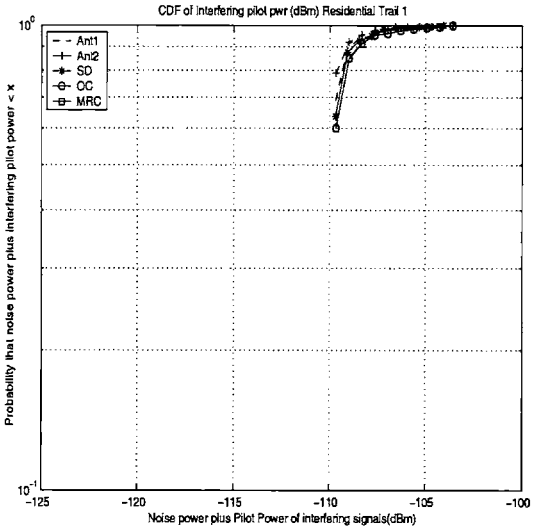

Figure 5-38: CDF of Intf. + Noise Power. Residential: handset on phantom head facing window

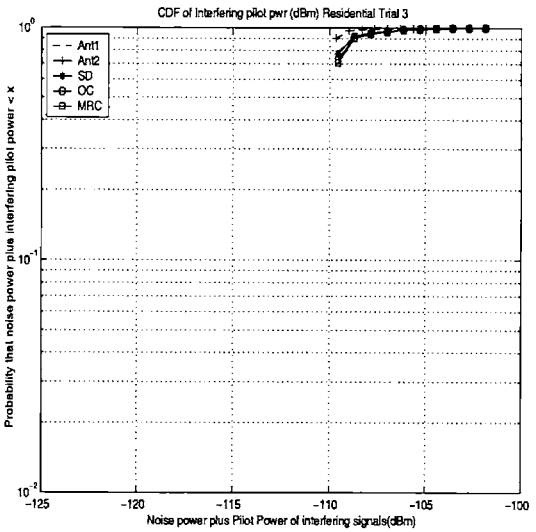

Figure 5-39: CDF of Intf. + Noise Power. Residential: handset held by human operator facing window

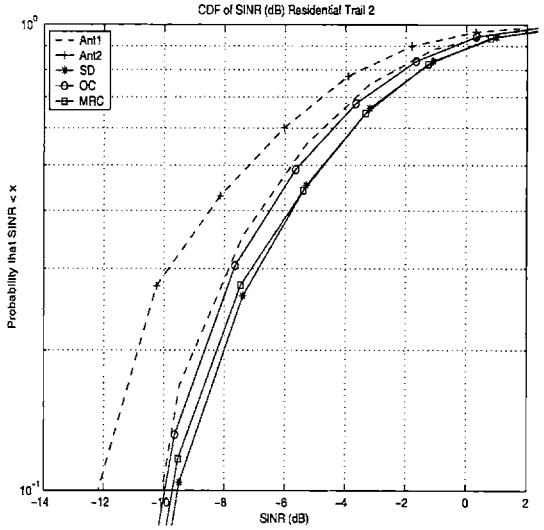

Figure 5-40: CDF of SINR. Residential: handset on phantom head facing inside

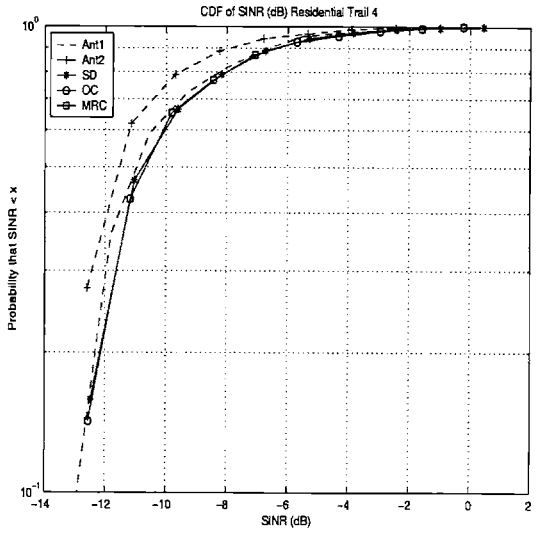

Figure 5-41: CDF of SINR. Residential: handset held by human operator facing inside

Table 5.9: SINR gain of open area trials with handset facing inside

	Human Operator		
Percentile	**SD**	**MRC**	**OC**
90	0.6	0.4	0.0

addition interference power is clearly below the 10^{-10} "noise term" added to $\mathbf{R}_{nn}$ and $\mathbf{R}_{MRC}$ matrices used in OC and MRC weight generation respectively. The very low SINR gains therefore made sense because the we should expect near 0dB SINR gains in the presence of white additive noise when the SINR of one antenna dominates that of the other antenna. In the presence of non-correlated white Gaussian noise, OC is equivalent to MRC; large power and SINR differences between the two antennas makes the dual antenna system become effectively a single antenna. As such SD selects the antenna with the stronger SINR value nearly all the time, and the MRC weights will be heavily in favor of the stronger antenna.

Handset facing inside

From table 5.9 at the 90%tile the SINR gain for SD and MRC is low but above 0dB; while that of OC is 0dB.

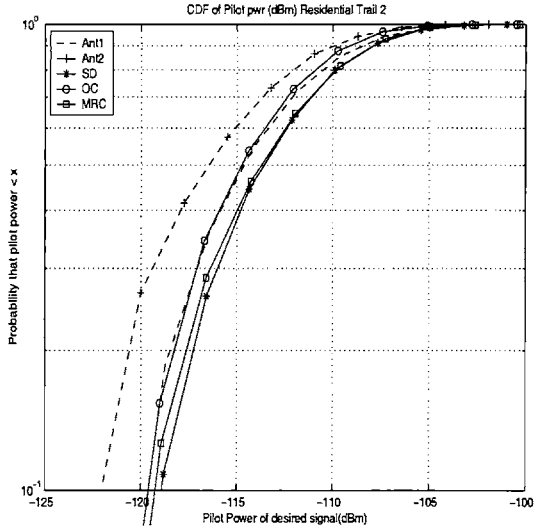

Figure 5-42: CDF of Desired Signal Power. Residential: handset on phantom head facing inside

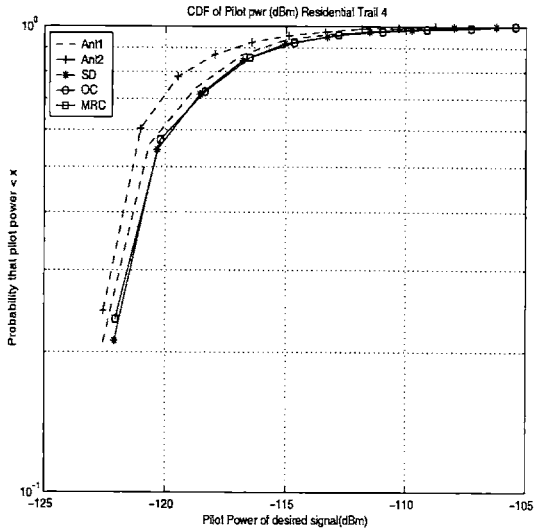

Figure 5-43: CDF of Desired Signal Power. Residential: handset held by human operator facing inside

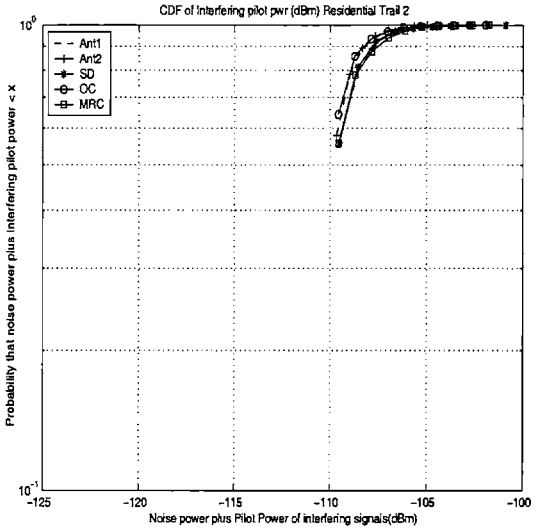

Figure 5-44: CDF of Interference and Noise Power. Residential: handset on phantom head facing inside

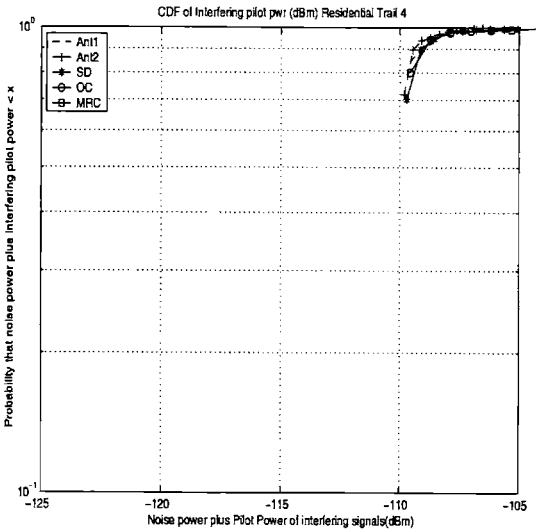

Figure 5-45: CDF of Interference and Noise Power. Residential: handset held by human operator facing inside

5.3 Summary of Results

The results obtained can be separated into two categories. One category is SINR gains using SD, MRC, and OC in an interference limited regime and another is in an noise limited regime where signal power itself is in the noise.

In the interference limited regime most of the OC SINR gains were also achievable using SD combining. SD gains were usually greater than 2.0 dB with the phantom head dummy. MRC SINR gains above the diversity gains were always below 0dB and ranged between -0.6dB and -0.4dB. OC SINR gains above the diversity gains were usually above 0dB and ranged from -0.2dB and 0.4dB. Limitations in OC weight-vector estimation leads us to expect higher OC and MRC SINR gains when more accurate methods are used to estimate the correlation matrices R_{nn} and r_{xd} and the MRC noise plus interference power matrix R_{MRC}.

In the noise limited regime SD, MRC, and OC SINR gains were low (below 1.0dB). For OC and MRC this may be accounted for by the fact that the actual noise power was not included in our estimation of MR and OC weights. Instead a 10^{-10} additive noise term was employed. The $\mathbf{R}_{nn}$ and $\mathbf{R}_{MRC}$ was, therefore, normally the identity matrix. MRC and OC SINR gains could have been higher had the actual noise powers been included. SD gains were also below 1.0dB because of the large difference in signal power on the two antennas (the top-monopole had stronger power for a large fraction of the time).

The effect of the human operator's hand on the dual handset antenna system considered is to affect the power received by the internal monopole. When the human operator holds the handset the power received by the monopole decreases relative to the top mounted monopole. This causes an increase in the power difference received by the two antennas and reduces the SD and MRC SINR gains. OC SINR gains are less affected by the operator's hand.

The effect of moving the handset from facing the window to facing the inside of the test van is to increase the power of the desired signal received by the internal

monopole. The power difference between the two antennas decreases and in general SINR gain of SD, MRC and OC increased.

Chapter 6

Report Summary and Suggestions For Future Work

In this thesis, the performance of a mobile handset with a top-mounted monopole and back-mounted internal monopole was determined in the field. Handset field tests were conducted both for the handset attached to a phantom-head model and held by a human operator so that the effect of hand blockage and coupling were measured. The measurements were made on the IS-95 (CDMA) SPRINT PCS system in various parts of San Diego. Logged data was analyzed for single antenna performance, SD, MRC and OC.

From the results it can be concluded that with smart antenna combining schemes implemented at the mobile handset forward link sensitivity improvements of up to 2.6dB are achieveable. When the mobile handset antennas were not blocked by the operator's hand and the mobile handset was in an interference limited region, 90% of the time, OC was able to provided up to 2.6dB SINR gains, SD provided up to 2.2dB SINR gains and MRC provided up to 1.6dB SINR gains. The difference between the more simple SD combining scheme and that of MRC and OC was not dramatic. MRC under-performed SD because the MRC-weight generation was inaccurate and to some extent interference was correlated at the two antennas. OC did not significantly

outperform SD because of inaccurate weight generation. When in a noise limited region OC, SD and MRC SINR gains fell to 0dB. The 0dB gains can be attributed to the particular handset design tested, which resulted in large power differences in received signals at the antenna terminals. Handset designs with closer spaced omni-directional antennas would not have such large signal power differences and should therefore be investigated.

The method used to generate the weights for OC and MRC combining was post-detection based and relied on approximations of the interference plus noise cross correlation matrix, and interference plus noise power. The cross correlation matrix, and interference plus noise power were approximated using the pilot weighted complex path gains. Limitations in the estimation accuracy of the pilot weighted path gains used to generate the MRC and OC weight vectors raise expectations for higher OC and MRC SINR gains than what was reported. A next step in OC combining in handset diversity antennas is, therefore, to improve the accuracies of weight-generation. Two approaches to increasing the accuracy of weight generation are considered in Appendix A

Appendix A

Methods for Increased OC Weight precision

This chapter proposed two ways of increasing the OC weight estimation. One method is post-detection based, while the other is pre-detection based. The two methods proposed require that the frequency error in the sampling clock be eliminated. The sampling clock's fluctuation was a result of the use of an internal sampling clock whose stability could not be maintained. The sampling frequency could be stabilized by using an external local oscillator to provide timing for the A2DC used in signal digitization.

Although attention is payed to OC weight estimation, the process can be adapted to increase MRC weight estimation. Figure A-1 shows the components of MRC and OC combining. The figure shows that pre-detection based methods can be used to improve the estimation accuracies in the Filter Section of the MRC and OC combiners. The Filter Section in OC is responsible for cross correlated interference plus cancellation. The EGC Equivalent Combiner Section would benefit from post-detection based methods.

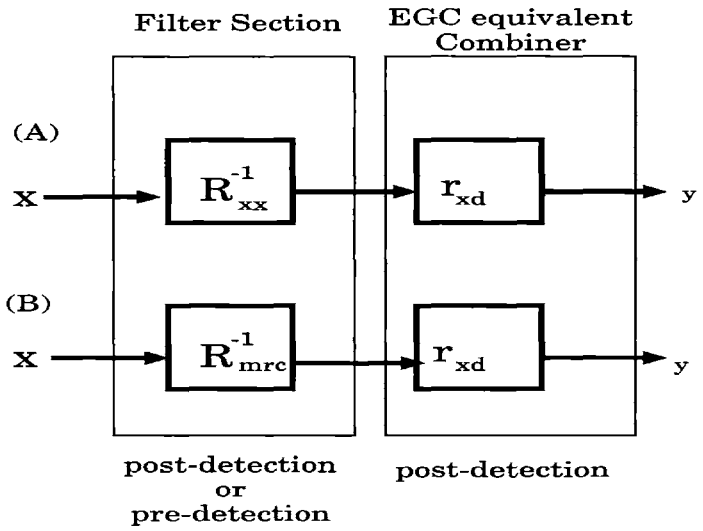

Figure A-1: Components of MRC and OC combiner

A.1 Post-Detection

The first approach to increasing accuracy is to continue using the complex fading coefficients to approximate the OC weights but to increase the resolution of the multi-path components to Chipx4 (4 times Chipx1) resolution. Thus two pilots with a delay of $\frac{1}{4}\frac{1}{1228800}$ can be distinguished. Use of an early late-gate mechanism concentrates the energy of the multi-path components into a single PN offset position, reduces pilot power smearing and increases the accuracy of the OC weights. An increase in the accuracy of the parameter estimation leads naturally to an increase in the OC SINR gains.

A.2 Pre-Detection

The second approach to increasing the accuracy in the OC weight generation, is to use the pre-detected digitized samples to generate the OC weight vector. If the sampling clock fluctuations can be eliminated, then the cross correlation matrix $\mathbf{R}_{xx}$ can be accurately calculated using the digitized samples. The OC weight vector $\mathbf{w} = \mathbf{R}_{xx}^{-1}\mathbf{r}_{xd}$ relation to can be used to generate the OC weights. In this scheme the $\mathbf{R}_{xx}$ matrix is

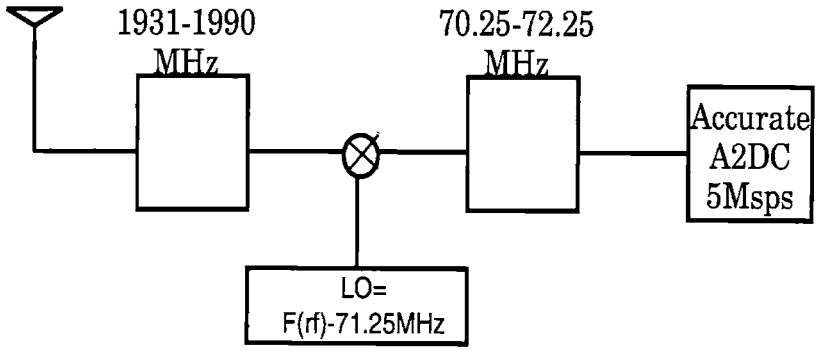

Figure A-2: Adapted system for to down-convert, digitize of RF signals

calculated using the digitized samples but the $\mathbf{r}_{xd}$ matrix is still calculated using the fading coefficients.

The first step requires a change in the system used to down-convert and digitize the RF signals illustrated in figure 4-5. The change involved mixing the 1931.25MHz signal down to 71.25MHz. The signal would be passed through 71.25Hz filter and sampled using an accurate 5MSps A2DC. The down-conversion and digitizing scheme is illustrated in figure A-2.

From figure A-2 the voltage at point (A), (B) and (C) are

$$r_{A,m}(t) = \Re\{n_m(t) + \sum_n \sum_i \beta_{i,n,m} e^{(j\omega(t-\theta_{i,n,m}))} s_n(t - t_{i,n,m})\} \tag{A.1}$$

$$r_{B,m}(t) = \Re\{n_m(t) + \sum_n \sum_i \beta_{i,n,m} e^{(j2\pi 71.25MHz(t-\theta_{i,n,m}))} s_n(t - t_{i,n,m})\} \tag{A.2}$$

$$r_{C,m}(k) = \Re\{n_m(k) + \sum_n \sum_i \beta_{i,n,m} e^{(j\frac{\pi}{2}(k-\theta_{i,n,m}))} s_n(k - t_{i,n,m})\} \tag{A.3}$$

Equation A.3 at antenna m can be split into it's odd and even time samples $k_o = \{1, 3, 5, ..\}, k_e = \{0, 2, 4, ..\}$. Note that the subscript (i, n) is dropped from the Walsh Functions even though the its alignments is dependent on the path i and sector n.

$$r_m(k_e) = \Re\{n_m(k_e) + \left(D_{0,m} + \sum_w D_{w,m} LONGCODEMASK_{w,m}\right) * \sum_n \sum_i \beta_{i,n,m} I_n(k_e) \cos(\theta_{i,n,m}) + Q_n(k_e) \sin(\theta_{i,n,m})\} \tag{A.4}$$

$$r_m(k_o) = \Re\{n_m(k_o) + \left(D_{0,m} + \sum_{w,m} D_{w,m} LONGCODEMASK_{w,m}\right) \sum_n \sum_i \beta_{i,n,m} Q_n(k_e) \cos(\theta_{i,n,m}) - I_n(k_e) \sin(\theta_{i,n,m})\} \tag{A.5}$$

Equation A.5 can be shifted down one sample to be in-phase with the even samples of A.4. Then we can simplify the products $r_1(k_e) * r_2(k_e)$ and $r_1(k_e) * r_2(k_o - 1)$ to

$$\begin{aligned} &r_m(k_e) * r_r(k_e) = \Re\{n_m(k_e)\}\Re\{n_2(k_e)\} + \\ &(D_{0,m} + \sum_w D_{w,m} LONGCODEMASK_{w,m})(D_{0,r} + \sum_w D_{w,r} LONGCODEMASK_{w,r}) \\ &\sum_n \sum_i \sum_p \sum_j \beta_{i,n,m} \beta_{j,p,r} \\ &(I_n(k_e) \cos(\theta_{i,n,1}) + Q_n(k_e) \sin(\theta_{i,n,1}))\,(I_p(k_e) \cos(\theta_{j,p,2}) + Q_p(k_e) \sin(\theta_{j,p,2})) \end{aligned} \tag{A.6}$$

$$\begin{aligned} &r_m(k_e) * r_r(k_o - 1) = \Re\{n_1(k_e)\}\Re\{n(k_o - 1)\} \\ &(D_{0,m} + \sum_w D_{w,m} LONGCODEMASK_{w,m})(D_{0,r} + \sum_w D_{w,r} LONGCODEMASK_{w,r}) \\ &\sum_n \sum_i \sum_p \sum_j \beta_{i,n,m} \beta_{j,p,r} \\ &(I_n(k_e) \cos(\theta_{i,n,m}) + Q_n(k_e) \sin(\theta_{i,n,m}))\,(Q_p(k_e) \cos(\theta_{j,p,r}) - I_p(k_e) \sin(\theta_{j,p,r})) \end{aligned} \tag{A.7}$$

As there is a 64 chip separation between pilot signals, it can be assumed that, when the average is taken, all terms for which $n \neq p$ reduce to zero. The expected value of

equation A.6 can be added to j times the expected value of equation A.7 to yield

$$\begin{aligned} &E\{r_m(k_e) * r_r(k_e) + jr_m(k_e) * r_r(k_o - 1)\} = \\ &E\{\Re\{n_m(k_e)\}\Re\{n_r(k_e)\} + j\Re\{n_m(k_e)\}\Re\{n_r(k_o - 1)\} \\ &\sum_n \sum_i \sum_j \beta_{i,n,m}\beta_{j,n,r} e^{j(\theta_{i,n,m} - \theta_{j,n,r})} E\{D_0^2 + \sum_w D_w^2 LONGCODEMASK_w^2\} \end{aligned} \tag{A.8}$$

Clearly, equation A.8 is in terms of the cross correlation matrix $R_{xx}(m, r)$ at indices m and r. Thus the cross correlation matrix does not need to be approximated using the pilot weighted fading coefficients: they can be calculated directly from sampled data. The cross correlation of the received signal with the desired signal, $\mathbf{r}_{xd}$ would still have to be estimated using the pilot weighted fading coefficients. So increased resolution (to Chipx4) of pilot signal detection is still required.

Bibliography

[1] *TA/EIA/IS-95A + TSB74: Mobile Station-Base Station Compatability Standard for Dual Mode Wideband Spread Spectrum Cellular System.*

[2] M[ario] Bonaccorso. *Optimum Combining in a CDMA High Data Rate Communication System.* PhD thesis, Industrial Thesis at Qualcomm Inc., 1999.

[3] Braun, C., Nilsson, M., and Murch, R. Simulation and measurement of the interference rejection capacity of handset. volume 49, pages 1068–1073, 1999.

[4] R. H Clarke. A statistical theory of mobile-radio reception. *Bell Systems Technical Journal*, pages 211–219, 1980.

[5] Colsburn, J. S., Rahmat-Sami Y., Jensen, M. A., and Pottie, G. J. Evaluation of personal communications dual-antenna handset diversity performance. volume 47, pages 737–746, 1998.

[6] R[ichard] B. Ertel. *Antenna Array Systems: Propagation and Performance.* PhD thesis, Virginia Polytechnic Insitute and State University, 1999.

[7] Gaggioli F. and Correia M. Assessment of diversity performance from measured data at the millimeter waveband. In *Vehicular Technology Conference*, volume 3, pages 1795–1799. IEEE, 1998.

[8] Tsunekawa K. Diversity antennas for portable telephones. In *Vehicular Technology Conference*, volume 36, pages 50–56. IEEE, 1989.

[9] Leather, P. S. H. and Parsons, J. D. Handheld antenna diversity experiments at 450mhz. pages 1–4, 1996.

[10] W[illiam] C. Y. Lee. *Mobile Communication Engineering.* dunno, 1981.

[11] W[illiam] C. Y. Lee. *Mobile Cellular Telecommunications Systems.* dunno, 1989.

[12] Sash, A. and Haimovich, A. Handheld antenna diversity experiments at 450mhz. pages 1–4, 1996.

[13] Vaughan, R[odney] G. and Anderson, J. Antenna diversity in mobile communications. In *IEEE Transactions on Vehicular Technology*, volume 36, pages 149–172. IEEE, 1987.